Simulating noncontact atomic force microscopy images

James R. Chelikowsky, Dingxin Fan, Alex J. Lee, and Yuki Sakai

Phys. Rev. Materials **3**, 110302 — Published 27 November 2019

DOI: 10.1103/PhysRevMaterials.3.110302

Simulating Non-Contact Atomic Force Microscopy Images

James R. Chelikowsky[a,b,c], Dingxin Fan[b], Alex J. Lee[b] and Yuki Sakai[a]

[a] *Oden Institute for Computational Engineering and Sciences*

[b] *Department of Chemical Engineering*

[c] *Department of Physics*

University of Texas at Austin

Austin, TX 78712

(Dated: November 6, 2019)

Abstract

A scanning probe with an atomically sharp tip is used in atomic force microscopy. As the probe is rastered over the specimen of interest, changes in its vibration mode can be ascribed to changes in the interatomic forces between the specimen and the tip. Various modes for implementing atomic force measures exist. One of the most successful modes is frequency modulation non-contact atomic force microscopy. Here, we address the role of replicating accurate forces on the probe tip to simulate images within this mode. We examine several approaches. One involves the use of classical force fields based on interatomic potentials, where the potentials are often fit to experiment. Other approaches center on the use of forces generated from quantum based calculations. We consider the development of a "virtual tip" approximation wherein the probe tip senses electrostatic forces generated by the specimen. This approach treats the specimen quantum mechanically, while the tip is treated as a classical object. We also consider the use of an embedding approximation to avoid direct computations of the specimen in the presence of the tip. In this method, the tip and specimen are treated quantum mechanically. However, the electronic structure of the specimen is computed in the absence of the probe tip. The electronic density of the specimen is then fixed and the electronic structure of the tip is then computed in the presence of the fixed density. As a general approach, we outline new methods for the full computation of quantum forces between the tip and specimen. We note that quantum based forces are particularly important as they directly contain the chemical nature of the forces present without the use of any adjustable parameters. We illustrate recent algorithmic developments to computing quantum forces that can produce accurate simulations of atomic force microscopy images for large and complex molecular species. We also suggest new pathways to overcome current challenges in this rapidly evolving field.

I. INTRODUCTION

Without accurate knowledge of the atomic structure of a material, understanding its properties is difficult, if not impossible. For this reason, a number of techniques to define and determine atomic positions have been developed. For example, the use of X-ray diffraction offers a mature technique for determining the atomic structure of a crystal. By carefully analyzing the diffracted beams with respect to their intensity and spatial distribution, a crystallographer can infer the atomic positions for a proposed crystal structure and in some circumstances the electronic charge distribution. With this information, one can determine a definitive crystal structure, including the composition of the crystal and internal structural information such as atomic coordination, including bond lengths and angles, and even the nature of the chemical bonds present. Molecular structures can also be determined by X-ray diffraction if the molecules of interest can be crystallized. For instance, the 1946 Nobel prize was awarded in part for crystallizing enzymes and the corresponding X-ray diffraction work to characterize their structure. A more recent example centers on the molecule C_{60}. The definitive structure of this molecule occurred when it was dissolved in benzene and made into a crystalline form. X-ray diffraction patterns were obtained and analyzed from the crystalline form. The analysis yielded the iconic buckyball structure for the constituent molecule [1, 2]. Before these X-ray measurements were made, the structure of the C_{60} molecule could only be inferred by indirect means, which led to contentious arguments at the time [3].

If the material cannot be crystallized, predicting the structure can be difficult, especially for isolated molecular systems. In contrast to X-ray diffraction measurements, scanning probe microscopy yields images that do not depend on the presence of crystallinity. In these measurements, a probe, which often consists of a sharp tip on a cantilever, is systematically swept over a specimen of interest [4–6]. Provided the probe tip is adjusted to be sufficiently close to the specimen to sense changes in some specified property, structural information can be obtained, albeit often in an indirect manner. For example, if a current is passed through from the probe into the specimen (or vice versa), small changes in the current can be detected as the probe is moved across the specimen. This operation is typified by *scanning tunneling microscopy* (STM) [7–9]. Another property is based on changes in the electrostatic forces between the probe tip and the specimen. If the cantilever is vibrating at

some resonant frequency, the change in force on the tip induced by the specimen can result in a change in the vibrating frequency as the probe is moved across the specimen. This operation is typified by *atomic force microscopy* (AFM) [10]. Collectively such microscopies are known as *scanning probe microscopies* (SPM).

Our focus is on atomic force microscopy applied to surfaces and molecular structures. This form of microscopy has achieved some remarkable and unprecedented results such as the subatomic resolution of the chemical bond. AFM work has been characterized as providing a "...completely new perspective for characterization of molecular systems on surfaces with unprecedented resolution. The possibility to image the internal chemical structure of individual molecules is a *dream come true*... " [6].

II. ATOMIC FORCE MICROSCOPY SETUP

Atomic force microscopy was originally designed to avoid a limitation of scanning tunneling microscopy. Measurements that involve current flow into, or out of, the specimen are difficult for insulators and often preclude scanning tunneling measurements. Atomic force microscopy does not suffer from this liability. AFM can image almost any type of surface, including polymers, ceramics, composites, glass, dielectrics, and biological specimens [4].

An illustrative setup for an AFM instrument is presented in Fig. 1. In this set up, a vibrating cantilever with a tip senses the sample. By setting the lock-in el fctronics to the fundamental frequency of the cantilever, small changes in the vibrational motion of the cantilever can be observed. Contemporary setups employ piezoelectric sensors as shown in the figure [11]. Other setups may employ optical means to measure frequency shifts. These elements aim to control accurate and precise movements of the scanning process both in terms of positioning the specimen and in driving the cantilever and accompanying tip [11–13].

There are different imaging modes in AFM. For example, the probe tip on the cantilever can come into contact with the sample in a "static mode" or remain above the specimen in a "dynamical or vibrating mode." Our focus is on the latter, known as "non-contact AFM (nc-AFM)." This mode has several advantages over other modes. Since the tip does not strongly interact with the specimen, modeling the system is easier as the tip can be viewed as a small perturbation on the sample. Moreover, this model does not suffer from tip or

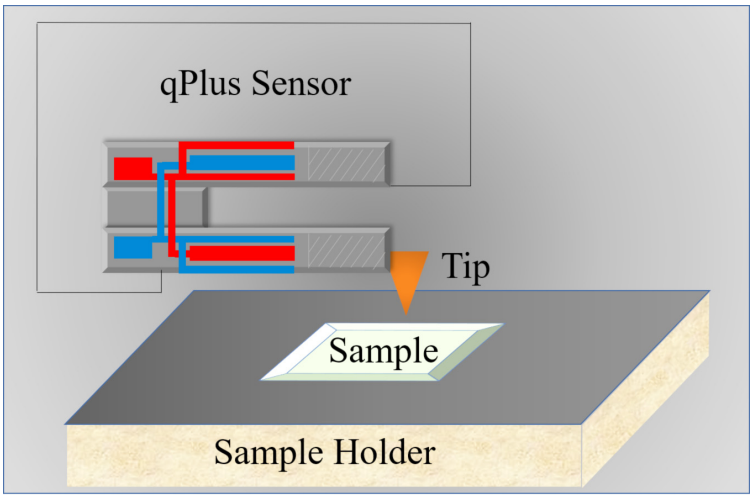

FIG. 1. Schematic diagram of atomic force microscope. As the tip mounted on a cantilever is rastered over the sample, a piezoelectric sensor detects changes induced by the sample on the vibrational motion of the cantilever.

sample degradation that can occur with "contact mode" measurements.

A common operating mode is to keep the vibrating tip at a constant height above the specimen and measure changes in the vibrational frequencies as the tip interacts with the specimen. The frequency of the vibrating tip can be measured with high sensitivity and permits the use of "very stiff" cantilevers. Such cantilevers provide stability near the vicinity of the surface. This technique provided the first atomic resolution images [4, 14].

A remarkable attribute of this instrumentation is that interatomic forces at the microscopic level can make macroscopic changes in the motion of the cantilever. In Fig. 2, an nc-AFM image is illustrated from the work of Gross *et al.* [15]. The molecule is a polycyclic hydrocarbon, hexabenzocoronene (HBC). The particulars of the chemical bond in the molecule are clearly articulated in the image. Even differences between bond order are apparent, along with bond distortions that offer insights into how the tip interacts with transverse forces [15–18].

The resolution of the images presented in Fig. 2 is not unique to this molecule. This instrumentation has resolved the chemical bond and bond order in a number of hydrocarbons [19–23]. Some workers have even claimed to have resolved hydrogen bonding between hydrocarbon molecules [24–27]. While our focus is often on hydrocarbons owing to its capability of discerning bond order, AFM can also be used to resolve the internal structure of a variety of systems, *e.g.*, metal clusters [28].

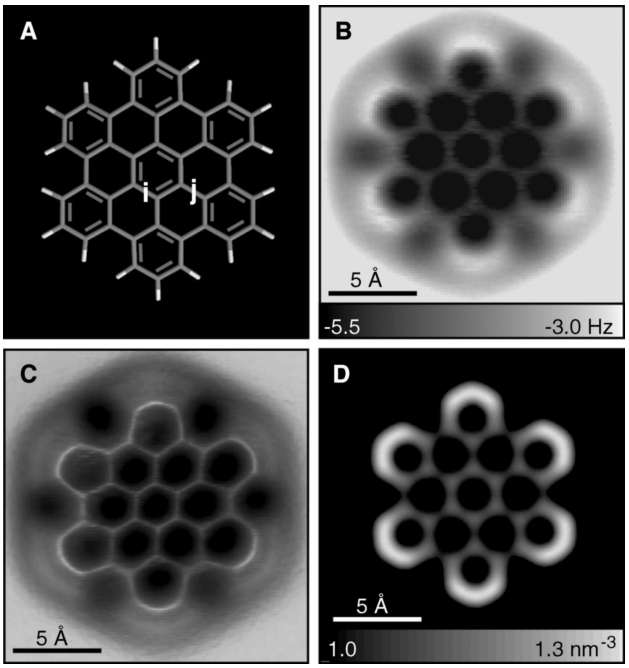

FIG. 2. Non-contact AFM images for the hexabenzocoronene (HBC) molecule. (A) Stick model. (B) Constant-height AFM measurements for an HBC molecule on a Cu (111) surface substrate. (C) A pseudo-3D representation that highlights the local maxima. (D) Calculated electron density above the molecular plane. From Gross et al. [15]

We note that an atomic force microscope possesses several advantages over other popular methods for determining surface structures. For example, methods using particle probes such as scanning electron microscopy (SEM) are diffraction limited, which complicates its use in obtaining atomic resolution. Suppose one wants to resolve a subatomic feature associated with the chemical bond. An electron with an energy of 10 keV possesses a de Broglie wavelength of about 0.01 nm, which is required to obtain atomic resolution. The control of such relatively high energy electrons is complex, *e.g.*, a vacuum environment is required, and exposing the specimen to high energy electrons may result in damaging the specimen.

Of course, AFM has some disadvantages when compared to SEM. The scanning speed and area covered with AFM is limited, although some advances in this area have been proposed [6, 29]. A major drawback of AFM centers on characterizing the tip. At the atomistic limit, details of the tip such as its shape, structure and composition are usually not known. Without such information, modeling forces on the tip is problematic.

III. THE THEORY OF ATOMIC FORCE MICROSCOPY

Figure 3 illustrates the interaction of a tip with a molecule on a substrate. The forces on the tip will alter its motion and be detected as shown in Fig. 1. A simple view of the process centers on changes in the motion of the tip in the presence of the specimen, and possibly the substrate.

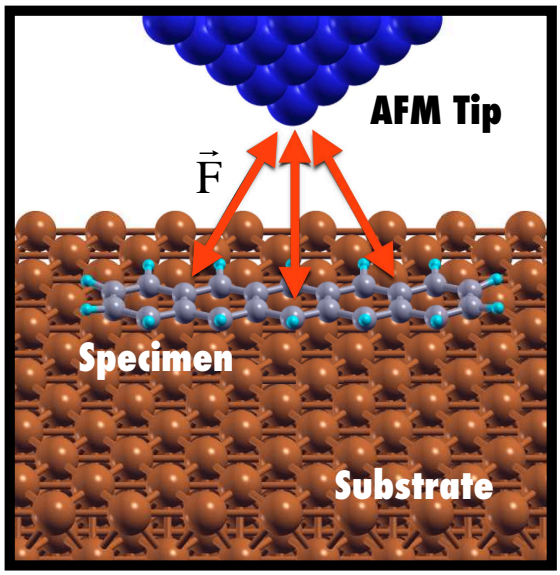

FIG. 3. Schematic of a nc-AFM tip probing a specimen molecule, pentacene, residing on a copper substrate. Forces between the specimen, the substrate and the tip will alter the vibrational mode of the tip yielding structural information about the molecule of interest.

We can treat the tip moving as a harmonic oscillator with some characteristic frequency [30, 31]. In Fig. 4, we quantify this picture by assuming a cantilever moving as a harmonic oscillator with an amplitude, A, and a nearest approach of the tip to the surface as d. We assume a z axis perpendicular to the surface. The position of the tip is given by

$$z(t) = d + A\cos(2\pi f_0\ t) \tag{1}$$

where f_0 is the resonant frequency of the tip in the absence of the sample. This frequency is given by

$$f_0 = \frac{1}{2\pi}\sqrt{\frac{k}{m^*}} \tag{2}$$

where k is the spring constant of the cantilever and m^* is the effective mass of the cantilever.

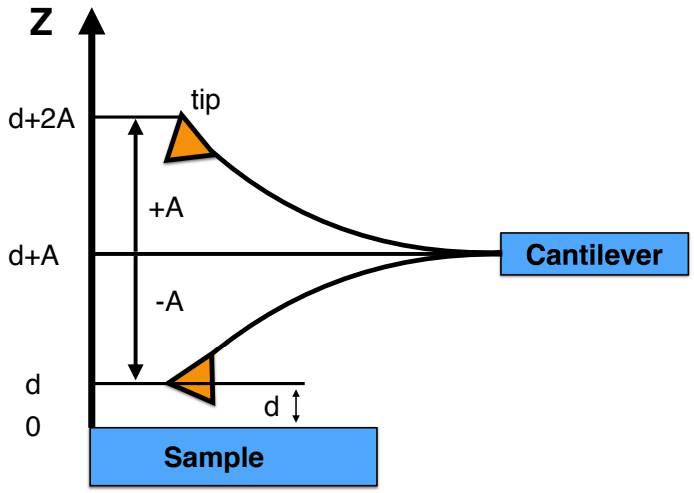

FIG. 4. Schematic of a nc-AFM tip moving with a vibrating cantilever. We assume the motion of the tip has an amplitude, A, and the nearest approach to the sample is d.

Suppose the role of the sample is to modify the intrinsic spring constant such that

$$k' = k + k_{ts} \tag{3}$$

where k' is the effective spring constant in the presence of the sample and k_{ts} is the effective change in the intrinsic spring constant. If the change were constant during the oscillation cycle, then

$$k_{ts} = -\frac{\partial F_{ts}}{\partial z} \tag{4}$$

We assume the force between the tip and sample is given by F_{ts} and acts perpendicular to the surface. The frequency shift can then be computed directly from:

$$\Delta f = f_0 \frac{k_{ts}}{2k} = -f_0 \frac{1}{2k} \frac{\partial F_{ts}}{\partial z} \tag{5}$$

This expression may look overly simplified, but it works quite well. A more rigorous approach is to average over the oscillation cycle:

$$\Delta f = f_0 \frac{< k_{ts} >}{2k} \tag{6}$$

This can be found from the following expression:

$$< k_{ts}(z) >= \frac{2}{\pi A^2} \int_{-A}^{A} k_{ts}(z - z') \sqrt{A^2 - z'^2}\, dz' \tag{7}$$

where z is the operating height of the AFM tip. (In Fig. 4, the operating height would be $z = d + A$.) The main contribution to the integrand occurs near the turning point of the cantilever oscillation, *i.e.*, when the tip is closest to the sample. In this case, the integral need not be explicitly performed as one can compute $-\partial F_{ts}/\partial z$ at the height of interest.

The tip-specimen forces can be mapped in terms of frequency shifts to produce an AFM image. There are two fundamental questions involved in simulating images: (1) Can we accurately predict or simulate the images? and (2) How do we interpret the images? These questions are closely coupled. If we cannot predict the images, then interpretation is problematic.

In general, SPM measures changes a specified property such as current or a vibrational frequency, and does not directly probe the atomic structure of specimen. This complicates interpreting the probe image.

In STM measurements an interpretative model exists from Tersoff and Hamann [32]. In its simplest form, we can write the measured tunneling current as follows:

$$I(\vec{r}, V) \propto \pm \sum_i \int_{E_f}^{E_f \pm V} |\psi_i(\vec{r})|^2\, \delta(E - E_i)\, dE \tag{8}$$

where V is the applied bias voltage, E_f is the Fermi level, ψ_i is an electronic state of the specimen within the allowed tunneling regime from E_f to $E_f \pm V$, *e.g.*, a filled state below the Fermi level for tunneling current out of the molecule, or an empty state above the Fermi for tunneling current into the molecule. Within this formalism, the tunneling current is proportional to the local density of states integrated over the energy range of interest. In this model, the tip is not explicitly considered. Rather, the tip wave function is assumed to be an "s-state" without specific structure.

This model can be used to analyze images and most importantly explains why the atomic positions may not correspond to regions where the tunneling current is enhanced. The ability to tunnel current into (or out of) a molecule depends on the spatial extent of an available empty (or filled) state. This can result in confusing the spatial extent of the wave function with the presence or absence of an atom. A notable example is the structure of Ag atoms on the Si (111) surface [33]. STM images correspond to contributions from empty surface

states near the Fermi level. These states are localized in regions between the Ag atoms, not coincident with the atomic positions.

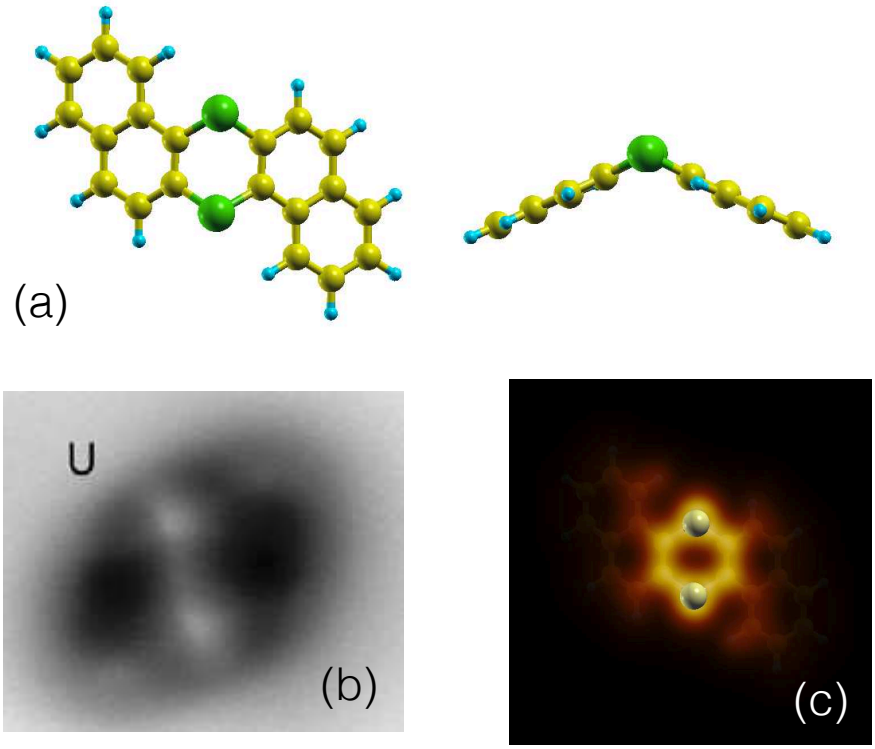

FIG. 5. (a) DBTH model with views of with upward-pointing sulfur atoms. The yellow, green, and cyan atoms represent carbon, sulfur, and hydrogen respectively. The left figure shows a top-down image. The right figure shows a side view. (b) Experimental image of DBTH from Pavliček et al. [34] The AFM image suggests an interaction, *e.g.*, a chemical bond, existing between the two sulfur atoms. (c) Electronic charge density for the DBTH molecule. The sulfur atoms are shown as spheres, the yellowish regions correspond to an enhanced charge density showing this existence of carbon-carbon and carbon-sulfur bonds and the absence of any sulfur-sulfur bonds.

Similar issues can occur in AFM imaging. The atomic positions need not be commensurate localized features in the AFM image that appear to replicate chemical bonds between atoms. We give an example for the dibenzo[a,h]thianthrene (DBTH) molecule. This molecule possesses two S apex atoms as illustrated in Fig. 5.

The image generated by nc-AFM suggests a "bond" exists between the apex sulfur atoms. Specifically, the two sulfur atoms appear as light colored circles with a light line representing

the bond-like feature between the sulfurs. This nc-AFM image contradicts the molecular model [Fig. 5(a)], in which no bond is expected between the sulfur atoms.

Electronic structure calculations also confirm that no bond exists between the sulfur atoms. In Fig. 5(c), the electronic charge density for this molecule is plotted in a plane passing through the sulfur atoms and parallel to a plane containing the nearest neighbor carbon atoms bonded to the sulfur atoms. If a bond exists between the sulfur atoms, this plane will capture its electronic charge density. No such contributions exist in Fig. 5(c). However, the expected bonds between the S atoms and the neighboring carbon atoms are clearly indicated by resulting charge density plot.

If one naively believed the nc-AFM, one could be misled into believing a S-S bond was present. As explained in the discussion below, the nc-AFM image can be related to strong changes in the electrostatic field, not the charge density. The electrostatic field shows strong changes between the S atoms as the electronic density goes through a local minimum between the S atoms. This large gradient of the density is reflected in the nc-AFM image.

Unfortunately, a simple model for interpreting AFM images remains elusive unlike the case for STM images. In particular, the computation of forces is complicated if the tip is explicitly included. A number of questions arise as to whether an AFM image can be interpreted without the explicit treatment of the atomistic structure of the tip as is often done in simulated STM images.

IV. COMPUTING INTERATOMIC FORCES

The determination of accurate interatomic forces is a key challenge for predicting the interaction of atomic species. Optimizing the structure of molecules or crystals, or running a molecular dynamics simulation, requires accurate forces. Simulating images in AFM also relies on determining accurate forces. The complexity of obtaining accurate forces is depicted in Fig. 3. The structure and chemistry of the tip, the specimen and the interaction of the specimen with the substrate can all add to the complexity of the problem.

Owing to the importance of interatomic forces, a number of approaches to computing them have been developed. Broadly speaking, there are two general approaches to calculating forces. One can implement atomic force fields, often based on model potentials fit to experiment, or fit to theoretical calculations. Or, one can compute interatomic forces di-

rectly from quantum solutions of the electronic structure problem. Each approach has assets and liabilities. Force field methods can be easy to implement and do not require extensive computational resources, generally speaking. Quantum forces need not be fit to experiment and include nonclassical effects. However, the computational load required can be demanding. If one were to remove the issue of computational loads, quantum forces are clearly the approach of choice. The inclusion of many body forces, chemically dependent interactions, charge transfer and hybridization in classical potentials is not transparent. The transcription of quantum mechanics into classical mechanics is often *ad hoc* and ill-defined. For similar reasons, contemporary molecular dynamics simulations center on the use of quantum forces, save situations where the computational load is insurmountable.

A key goal of work in this area is to simplify this problem to reduce the computational load, while not losing the ability to have accurate forces. Examples of such simplifications could include: (1) constructing classical force fields to avoid quantum calculations, but retaining sufficient accuracy to capture the essential features (2) treating the probe tip as a classical object with no explicit structure to remove issues involved with the microscopic structure of the tip (3) freezing the specimen electron density to separate quantum computations for the tip and for the specimen or (4) implementing new high performance algorithms to address large scale electronic structure problems. We will illustrate all of these approaches.

The probe tip can experience forces that arise from a variety of sources. These tip-sample forces are often loosely characterized as dispersion, covalent, ionic, electrostatic, metallic, magnetic, and so on. While most workers understand and agree on such characterizations, the use of the expression "Pauli forces" merits clarification. Consider the interaction of two inert gas atoms, say Ne atoms. At short distances, the Ne atoms will experience a strong repulsive force. The origin of this force arises from the Pauli exclusion principle. This force is "short-ranged." Yet, forces present between atoms separated by several bond lengths are sometimes termed "Pauli forces" in the AFM literature [35, 36]. However, the truly long range forces observed in nc-AFM are not repulsive as Pauli forces would be. The origin of such attractive forces is usually from van der Waals-like interactions [37–39]. A good discussion of this issue is presented elsewhere [35, 36].

A. Classical forces

There are several avenues open to quantifying the computation of forces between the tip and the sample to simulate the frequency shift of the probe tip. The simplest approach is to construct classical force field model either fit to experiment or fit to theory. A number of force fields are available in the literature and in databases [40–42].

In the case of nc-AFM wherein the tip only weakly interacts with the sample, one might ignore any redistribution of atomic positions, and possible changes in the nature of the chemical bonds present. In principle, the computational load in obtaining classical forces is tractable, and often doable even with limited computational resources.

However, a number of issues remain. In general, the morphology of the tip at the atomic scale is not known. Without this knowledge, the problem of simulating an image of specimen can be complicated. Often, the sensitivity of the image is tested through the use of a number of structural models for the probe tip.

When computing the forces between the tip and simple, a general approach is to decompose the total force as

$$\vec{F} = \vec{F}_c + \vec{F}_{dis} + \vec{F}_{chem} \tag{9}$$

where $\vec{F}_c$ is a long range electrostatic or coulombic force, $\vec{F}_{dis}$ is a dispersion force and $\vec{F}_{chem}$ is a short range chemical force arising from covalent, metallic or ionic bonding [43]. This separation may be useful in developing a physical picture of the nc-AFM image, but division of the total force into various components is clearly arbitrary.

The coulomb forces can be characterized by residual charges on the tip or specimen, or to an applied voltage between the tip and the specimen. For the purposes of our discussion, we will assume the lack of any applied voltage.

The dispersion forces can be obtained from a Van der Waals potential:

$$V_{vdw}(R_{ij}) = -E_o \left((\frac{\sigma}{R_{ij}})^{12} - (\frac{\sigma}{R_{ij}})^{6} \right) \tag{10}$$

where E_0 is a measure of the strength of the interaction, R_{ij} is the distance of between the interacting atoms (i, j), and σ is a measure of the length scale. By summing over all relevant atoms in the tip, specimen and substrate, the net interaction energy can be calculated as a function of the tip height. The change in this energy with position will yield the required

forces.

Chemical forces can be treated in a simple manner. Typically a Morse potential can serve as a useful starting point [43]:

$$V_{chem}(R_{ij}) = V_o \left(\exp(-2R_{ij}/\lambda) - 2\exp(-R_{ij}/\lambda)\right) \tag{11}$$

where the strength of the potential is given by V_0 and the potential range by λ.

In Fig. 6(a) experimental nc-AFM images of KBr by Ruschmeier *et al.* are illustrated [44]. As expected, atoms corresponding to K^+ and Br^- ions are readily identified. Most of the charge should be localized on the Br^- ion, so it is relatively easy to differentiate between the K^+ and Br^- sites. Fig. 6(b) clearly illustrates that K and Br atoms can be respectively seen as a minimum and maximum of the frequency shift profile when z is lower than 0.5 nm.

The authors analyzed forces on the tip using interatomic potentials to generate classical force fields. Ionic surfaces are prime candidates for simple potentials. The surfaces do not strongly relax or reconstruct, and the dominant forces for ionic interactions are pairwise, unlike covalent forces. There are a number of AFM studies for ionic forces in the literature [45–49].

The surface was modeled by taking a slab geometry with surface of interest exposed. The atomic geometries were also relaxed using interatomic potentials, although that is not a necessary step as the structure of a bulk crystal is usually known.

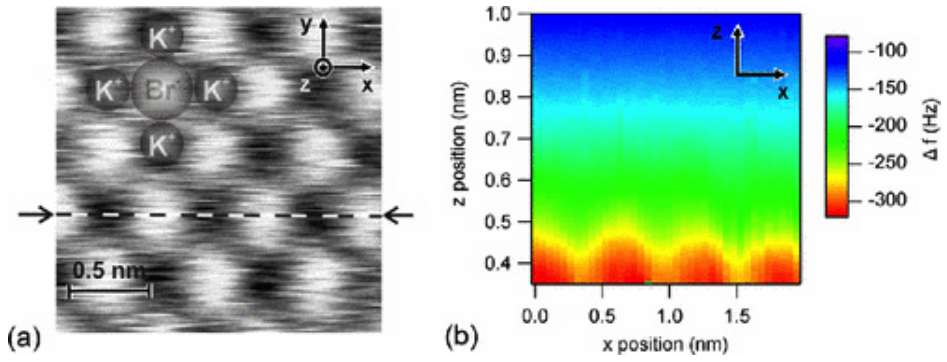

FIG. 6. (a) Surface topography of a KBr(001) sample measured at a constant frequency shift, indicating the position of K^+ and Br^- surface ions according to a force field analysis. The dashed line indicates a representative y position along the sites of topography maxima at which the force field measurements were performed. (b) Measured frequency shift versus relative tip-sample distance as a function of the horizontal tip position along the x axis. This work is from Ruschmeier, Schirmeisen and Hoffmann [44], experimental details can be found therein.

Modeling the tip can be more difficult and somewhat speculative. In the example we present here, the authors had earlier "crashed the tip" in the sample. The resulting images improved, most likely by creating a tip terminated by a fragment of the sample [44]. The authors considered a small nanocrystal, $(KBr)_{32}$ to model the tip. Given the lack of any detailed information, this is not an unreasonable approach. The model tip was relaxed using classical interatomic potentials and terminated with either the cation or anion. Simulated images were then created to assess the differences in the tip geometries.

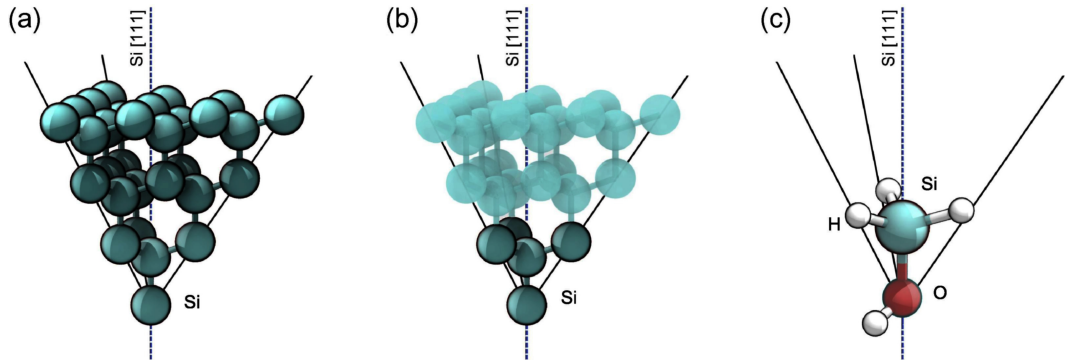

FIG. 7. Model structures for an AFM tip made of silicon and molecular model. (a) A large segment of crystalline silicon with an atomistically sharp tip. (b) Similar tip, but with fewer atoms. (c) Molecular analog of the tip. From Sanna, Dues and Schmidt [50].

Since the probe tips are often made from silicon, models of the tip based on crystalline silicon are often used as illustrated in Fig. 7. In terms of classical forces, the number of atoms in the tip do not represent a computational limitation. For quantum forces, the number of atoms do make a difference. The difference between the tip in Fig. 7(a) and 7b, could represent more than an order of magnitude in computing time. As a consequence, small molecular fragments are used whenever feasible to model the tip.

B. Quantum forces

In principle, accurate quantum derived forces can be extracted using electronic structure codes. One can solve for the total energy of the system on a grid above the specimen and take numerical derivatives to obtain the forces required for simulating AFM images. An alternative is to use the Hellmann-Feynman theorem. Since we need to raster the tip over the specimen to generate an image, it is straightforward to generate the energy surface and take numerical derivatives.

a. The Kohn-Sham equation. Two physical approximations have significantly advanced our ability to find a practical approach to solving the electronic structure problem. (1) Fixing the energy and length scales of the problem by focusing on the chemical active electronic states. The periodic table categorizes elements by the number of chemically active valence electrons. This physical realization can be included in developing algorithms that focus solely on these electronic states. The chemically inert electrons or core electrons, which do not contribute to the bonding process can be removed by the introduction of a potential that only binds the valence states. This potential, called a *pseudopotential*, allows one to use a simple description of the states wherein an atom like Pb with 82 electrons is no more difficult to handle than an atom like C with 6 electrons, as both atoms have 4 valence electrons [51–54]. (2) Mapping the all-electron problem to a one-electron problem. Walter Kohn received the 1998 Nobel Prize in Chemistry for developing "density functional theory (DFT)," which uses the electron density to construct an effective one-electron theory [55–57].

The combination of pseudopotentials and DFT results in the *Kohn-Sham eigenvalue equation*:

$$\mathcal{H}\psi_n(\vec{r}) = \big[\frac{-\hbar^2\nabla^2}{2m} + V_{ion}^p(\vec{r}) + e\int \frac{\rho(\vec{r}')}{|\vec{r}-\vec{r}'|}\, d^3r' + V_{xc}[\rho]\big]\psi_n(\vec{r}) = E_n\psi_n(\vec{r}) \qquad (12)$$

where $\mathcal{H}$ is the Hamiltonian, $\hbar$ is Planck's constant, m is the mass of the electron, e is the electronic charge, V_{ion}^p is the ionic pseudopotential (corresponding to the electron-nuclear interaction), ρ is the electronic density, V_{xc} is the effective potential for exchange-correlation, and (E_n, ψ_n) is the eigenpair for the orbital energy and corresponding wave function. ρ is given by

$$\rho(\vec{r}) = e\sum_{n,occup} |\psi_n(\vec{r})|^2 \qquad (13)$$

where the sum is over the occupied states. The effective potential V_{xc} is a functional of ρ. In general, V_{xc} is unknown. However, it can be computed in the limit of a homogeneous electron gas and applied to realistic systems under the assumption that the functional is "universal." The Kohn-Sham equation is solved self-consistently by initially taking ρ to be a superposition of atomic densities, which can easily be obtained for spherically symmetric, isolated atoms. The Kohn-Sham equation can yield accurate solutions for the energetic and spatial distributions of the electronic states of molecules, clusters, liquids and solids across a

wide range of length scales and for many weakly correlated systems. Using this information, one can predict materials properties such as phase stabilities– and optical, dielectric, and magnetic response functions without resort to experiment.

b. Solving the Kohn-Sham Equation. The Kohn-Sham equation, while sufficiently accurate for making useful predictions can be computationally intensive. To reduce the computational load, workers have focused on improving algorithms and capitalizing on advances in hardware. One traditional approach to solving the Kohn-Sham equation is to expand the wave functions in a basis, *e.g.*, plane waves, or linear combinations of atomic-like orbitals, *e.g.* Gaussians. The combination of a plane-waves basis and pseudopotentials is one of the most popular methods for determining the electronic and structural properties of materials owing to its ease of implementation and the simplicity of the method.

Another approach to the problem is to use *real-space* methods [58–63]. A real-space mesh approach to this problem is frequently the one of choice. This approach allows the use of state-of-the-art algorithms, which utilize sparse-matrix linear algebra for massively parallelized solutions of large systems. These new methods are mathematically robust, very accurate and well suited for modern, massively parallel computing resources [58–63].

For AFM applications, real space methods are easy to implement. For example, a confined systems such as an isolated molecule in the presence of a probe tip can be contained within a spherical domain [64, 65]. A cubic grid can be laid out and the Kohn-Sham equation can be discretized over the mesh. Higher order finite difference expressions can be used to express the Laplacian operator. This results in a large, but extremely space matrix for the Hamiltonian operator. This matrix need not be explicitly stored.

A key aspect of this approach is the development of efficient eigensolvers, which in the case at hand focus on sparse matrices. Such eigensolvers do not solve the problem eigenstate by eigenstate, but rather extract a subspace that spans the energy space of merit [60]. The subspace is created by the repeated application of the Hamiltonian expressed as a filtering polynomial. This method can dramatically reduce the computational load in some cases by an order of magnitude or more. These methods have allowed large systems with hundreds, if not thousands of atoms, to be explored [58–63].

Despite these advances, quantum solutions for forces can remain computationally intense as the forces need to be computed over a mesh of points to extract the AFM image. Specifically, we might need to solve for a thousand atom system over thousands of grid points.

Moreover, the Kohn-Sham equation scales poorly with respect to the number of electrons in the system, *i.e.*, if N is the number of desired eigenvalues, the computational time scales as N^n where $n \approx 2.5$ [59]. In such cases, generating an AFM image for a large specimen might remain beyond the capability of contemporary computational platforms.

Owing to the system size involved in solving for the forces, which includes atoms in the tip, the specimen and the substrate, simulating an AFM image of the entire specimen by solving the Kohn-Sham equation can be computationally demanding. Workers often consider computing forces along high symmetry lines of the system to reduce the computational loads.

While computational intensive, the procedure for computing forces is rather straightforward. One can compute the energy as a function of position of the tip and simply take the required derivatives to obtain the forces. Since one has to solve for the forces on a grid, the cost of computing derivatives by finite differencing the energies is low.

A important factor in simulating the tip-specimen interaction can be the presence of lateral forces that affect details of the tip orientation and have been shown to alter the image details. An example of this issue may be found in previous work on the molecule, C_{60} [15] and is illustrated in Fig. 8. Within this study, the tip is modeled by a CO molecule bonded to two Cu atoms with the C atom attached to the Cu atoms and the O atom directed to the C_{60} molecule. The tip is moved over a six fold ring on the top of the molecule as illustrated in Fig. 8C. The model seems naive by assuming the probe can be captured by an isolated CO molecule attached to the tip. However, without additional information, this is a reasonable approach.

The C_{60} molecule is composed of five and six membered rings. Calculations show that the bonds shared by six-fold are nominally "double bonds" and bonds shared by adjacent six fold to five fold membered rings are "single bonds." This is illustrated in a density functional computation in Fig. 8B wherein the valence charge density of the molecule is illustrated. Bonds listed by p and h in the figure exhibit a different charge density with the charge density more localized on the double bond h. The change in the energy of the system can be computed as the tip traverses the C_{60} molecule.

As the tip is moved across the specimen, atomic forces may alter the structure of the tip. For example, the orientation of a molecule bound to the tip might change when interacting with the substrate or specimen. The importance of the tip relaxation effect is also argued in simulations with classical Lennard-Jones potential [66]. However, the relaxation requires

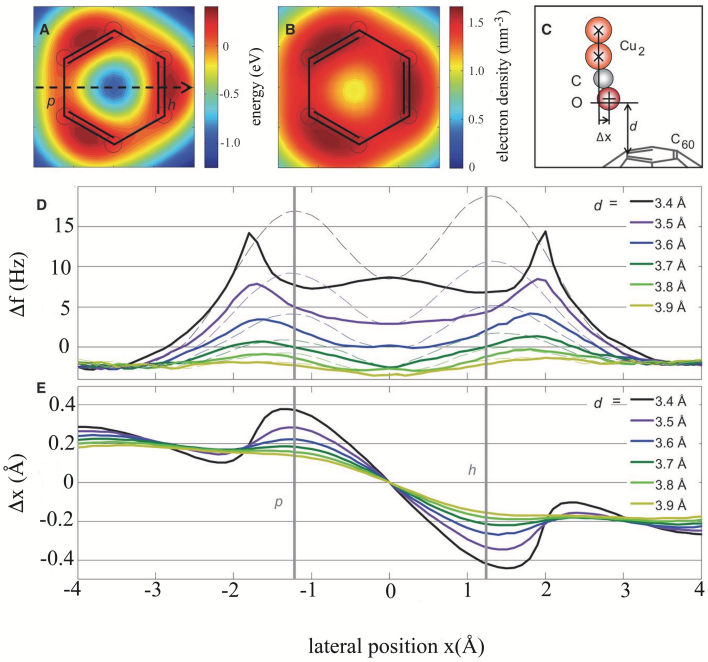

FIG. 8. Density functional theory calculations for the C_{60} molecule. Calculated interaction energy between the CO tip and C_{60} at d = 2.9 Å (A) and electron density (B). Using the tip model shown in (C), $\Delta f(x)$ line profiles along the dashed arrow in (A) were calculated with (solid lines) and without (thin dashed lines) relaxing the tip geometry, respectively (D). The relaxation resulted in a lateral displacement of the oxygen atom $\Delta f(x)$, as shown in (E). The vertical gray lines in (D) and (E) indicate the positions of the p and h bonds as expected from the atomic model. From Gross *et al.* [13].

tens of total energy calculation at each AFM grid point, and could not be practical in a routine first-principles AFM simulation. Guo *et al.* alternatively proposed a simple but useful approximation to include the tip relaxation effect in AFM [67]. This approximation assumes that the lateral displacement of a flexible tip is proportional to the lateral force acting on the tip ($\vec{F}$), i.e., the displacement [$\vec{\Delta}_{\rm lat}$, see Fig. 9(a)] of the end atom is given by

$$\vec{\Delta}_{\rm lat} = \frac{\vec{F}_{\rm lat}}{k_{\rm lat}}, \tag{14}$$

where $k_{\rm lat}$ represents the lateral stiffness of the tip. Here the vertical displacement caused by the relaxation effect (Δz) is generally negligibly small. The total energy is computed at the displaced atomic positions by interpolating a two-dimensional tip-sample interaction

energy map. This method is useful because it requires only "post-processing" of the existing AFM simulation data. This tip-tilting correction was applied to simulate the CO tip over a C_{60} molecule [67]. The simulated AFM image (force map) shown in Fig. 9(b) captures the distortion of the apparent image, as in the case of the fully relaxed tip. The simulated difference (25%) in the two apparent bond lengths of p and h agrees with the experimental value (30%) by using this approximation. In addition, the simulated AFM image of a pentacene molecule with the correction shows sharper apparent bond and distorted structure, which improves the agreement with the experimental image. In a moderate tip-sample distance region, this method should be a reasonable approximation to the tip relaxation effect.

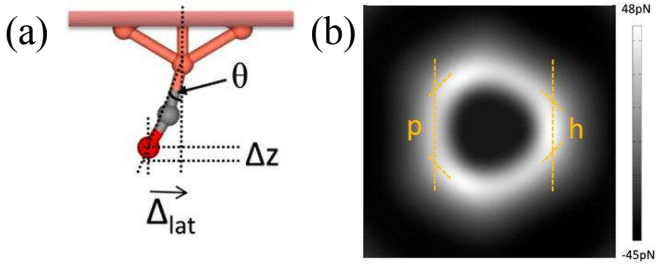

FIG. 9. (a) Schematic figure illustrating the tip relaxation effect. (b) Two-dimensional map of the force acting on a CO tip simulated over a C_{60} molecule. The tip tilting correction is applied. The definition of labels p and h is the same as that in Fig. 8. Reproduced from Ref. [67].

In principle, one could model the tip by explicitly including the functionalized tip and determining the motion of the molecular species involved while moving the tip. Such molecular dynamics methods would allow for the natural evolution of structural and electronic properties of the tip. A few approaches along this avenue have been attempted, albeit without an explicit quantum computation [68, 69].

V. AFM SIMULATIONS WITH VIRTUAL TIP METHOD

One promising method to avoid the particulars of the probe tip is to mimic its behavior with a classical, virtual tip. This is perhaps the simplest procedure beyond interatomic potentials and one which dramatically reduces the computational loads relative to full quantum computations. The essential idea is the same as used in simplifying the scanning tunneling microscopy configuration, *i.e.*, the atomistic details of the tip are removed from the

simulation.

The tip-sample force F_{ts} is calculated by a multipole expansion of the tip-sample interaction [70]. By treating the influence of the sample on the cantilever tip as a perturbation, the tip-sample interaction energy can be written as:

$$E_{ts}(\mathbf{r}) = \int |\phi(\mathbf{r}' - \mathbf{r})|^2 V_{ts}(\mathbf{r}') d\mathbf{r}', \tag{15}$$

where $\mathbf{r}$ is the position of the cantilever tip, V_{ts} is the potential on the tip due to the sample, and ϕ represents the electronic state of the tip, *e.g., the outermost orbital.* The expression assumes that the cantilever tip does not affect the structural and the electronic properties of the sample surface. The theory is applicable to simulate topography images, but not dissipation images. The tip-sample force can then be evaluated by:

$$\begin{aligned} F_{ts}(\mathbf{r}) &= -\nabla E_{ts}(\mathbf{r}) = -\nabla V_{ts}(\mathbf{r}) - \nabla(\nabla V_{ts}(\mathbf{r}) \cdot \int |\phi(\mathbf{r}' - \mathbf{r})|^2 (\mathbf{r}' - \mathbf{r}) d\mathbf{r}') \\ &= -\nabla V_{ts}(\mathbf{r}) - \nabla(\nabla V_{ts}(\mathbf{r}) \cdot \mathbf{p}) = -\nabla V_{ts}(\mathbf{r}) - \alpha \nabla(|\nabla V_{ts}(\mathbf{r})|^2) \end{aligned} \tag{16}$$

where the first line follows by expanding the potential V_{ts} around the tip position $\mathbf{r}$ up to first order. $\mathbf{p}$ is the polarization of the tip. Up to first-order, the polarization of the tip is linearly related to ∇V_{ts} by its polarizability α.

The first term of the resultant expression is the monopole term for the electrons present in the tip. For an electrically neutral system, there is a corresponding term with an opposite sign owing to the positively-charged ions. In nc-AFM experiments, long-range interaction owing to surface charges and tip-sample potential differences are usually removed by applying a tip-sample bias to enhance resolution.

The first non-zero leading term is the dipole interaction:

$$F_{ts}(\mathbf{r}) \propto -\nabla(|\nabla V_{ts}(\mathbf{r})|^2). \tag{17}$$

V_{ts} is taken to be the electrostatic part of the self-consistent potential (the Hartree potential and the local part of the ionic pseudopotential) of the sample from a first-principles calculation. The simulation cell does not include the cantilever tip. The polarizability, α, characterizes the structural and electronic properties of the cantilever tip, but its evaluation is not required as we are normally interested in relative frequency shifts.

The tip-sample force, F_{ts}, is calculated by Eqn. 17 numerically on each grid point, once a solution of the electronic structure is known. Using Eqn. 5, the frequency shift of the cantilever tip can then be evaluated by specifying the vibration amplitude A. A nc-AFM image is the height profile of the cantilever with constant frequency shift. In most studies, A is kept between 0.2 to 2 Å. The average tip height is adjusted to best fit the resolution of experimental images.

Within this simple approach, the "chemistry" of the tip is omitted; the role of tip functionalizations are not captured in any detail. Still, the method works well for many systems and provides one the ability to make a quick assessments of different structural models. In particular, the method requires only one computation: a solution of the electronic structure for the specimen of interest and the corresponding electrostatic field. No other approach offers less computation while incorporating the orbital character of the specimen.

The case of the Ag/Si(111) $\sqrt{3} \times \sqrt{3}$ $R30°$ surface provides a nice example [70]. The surface reconstruction can be described by the honeycomb-chained trimer model [71] which consists of a Si(111) substrate with a missing top-layer. The top layer is replaced by Ag trimers with the centers of the trimers forming a honeycomb network. A simulated image is shown in Fig. 10.

If the tip is close to the surface, each bright spot corresponds to the location of a Ag atom. By pulling the tip further away from the surface by 4 Å, there is a contrast change and the bright spots are shifted to the center of the Ag trimers. The virtual tip model in this example, allows one to distinguish contributions to the AFM image resulting from atomic positions and interstitial regions. Similar contrast changes with tip height had also been observed in experiment [72]. The result also agrees with a first-principles simulations [73] where the AFM probe tip was explicitly included in the simulation cell.

VI. FIRST-PRINCIPLES AFM SIMULATIONS WITH QUANTUM FORCES

A. Simulating the AFM image of organic molecule with functionalized tip

Since the first report on the subatomic resolution of the AFM image of a pentacene molecule [74], the visualization of the molecular structure by using a CO-functionalized tip is a key topic in the AFM research [75, 76]. Figs. 11(b) and 11(c) show experimental

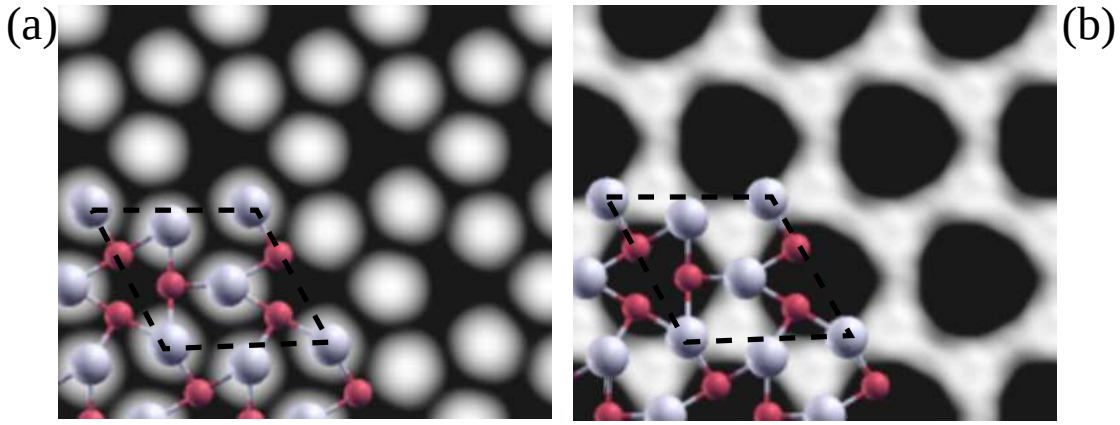

FIG. 10. Simulated nc-AFM image of the Ag/Si(111)-($\sqrt{3} \times \sqrt{3}$)$R30°$ surface with an average tip height of (a) 4 Å and (b) 8 Å respectively. The bottom left of the image is overlaid with the top Ag(gray) and Si(red) atoms of the honeycomb-chained trimer model. The ($\sqrt{3} \times \sqrt{3}$) unit cell is indicated.

AFM images of a dibenzo(cd,n)naphtho(3,2,1,8-pqra)perylene (DBNP) molecule with Xe-terminated and CO-terminated tips, respectively. [See Fig. 11(a) for the structure of the molecule.] The image with a CO-functionalized tip clearly shows higher resolution compared with that obtained with a Xe-terminated tip. Simulating AFM images of organic molecules is an important challenge for understanding the origin of the high resolution and the role of tip functionalization in AFM imaging [77–82].

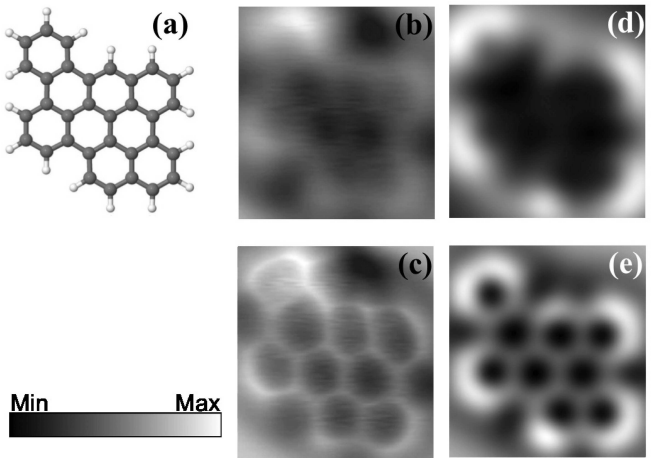

FIG. 11. (a) Ball-and-stick model of a DBNP molecule. Gray and white spheres represent carbon and hydrogen atoms, respectively. Experimental AFM images of a DBNP molecule taken with (b) Xe and (c) CO terminated tips. Simulated AFM images of a DBNP molecule with (d) the virtual tip method and (e) DFT-based method. Figures (a), (d), and (e) are from Ref. [83] and (b) and (c) are from Ref. [84].

As much as one would like to avoid details of the tip, there are circumstances where such an approach is not possible. In spite of its successful application to semiconductor surfaces, the virtual tip method cannot reproduce the AFM images of organic molecules measured with a CO functionalized tip versus a Xe tip. Fig. 11(d) presents the simulated AFM image of the same molecule by using the virtual tip method [83]. The edge structure of the molecule is seen in this simulated image, but the "inner structure" is barely recognized. Some improvement of the resolution in a simulated image can be obtained by adding a "quantum effect" to the virtual tip method. In particular, some workers have included the exchange-correlation contribution of the sample to the probe tip [85]. Of course, such an inclusion contradicts a classical description of the tip, but this approach remains computationally simple. Since the exchange-correlation addition depends solely on the specimen charge density, the chemistry of the tip is not considered.

The inner structure of the DBNP molecule is notably reproduced when the force acting on the tip is computed using DFT as shown in Fig. 11(e). The explicit modeling of the tip and the force calculations based on DFT computations are necessary to quantitatively simulate images using a CO-functionalized tip. Similar studies reinforce the need for including the chemistry of the tip. For example, single walled nanotubes cannot be quantitatively reproduced using pairwise Lennard-Jones potentials [86, 87].

Given the success of the first-principles simulations to experiments using functionalized tips, the role of the functionalization mechanism has been studied using DFT-based simulations [17, 35, 88–93]. Xin *et al.* reported computational experiments on various tip functionalization [89]. Figs.12(b) and 12(c) show the force line profile of a napthalene tetracarboxylic diimide [NTCDI, see Fig. 12(a)] molecule using various molecules as a tip. Here the profile is taken over the nitrogen and oxygen atoms [black dashed line in Fig.12(a)]. In Fig.12(b), all lines have only one peak at the nitrogen atom, and the neighboring oxygen atom is seen as a shoulder-like feature, except for the Au_2CO molecule case (the black line). This result suggests that the atomic resolution cannot be achieved when the end atom (*i.e.*, the atom close to the sample) is fluorine, silicon, phosphorus, sulfur, or xenon. On the other hand, the three atoms are clearly resolved in Fig.12(c) where the end atom is carbon, nitrogen, or oxygen. In addition, the CH_3CN (pink line) and HCN (blue line) tip yield almost identical results, indicating that the end atom is considered to be the dominant factor of the resolution in acquired AFM images.

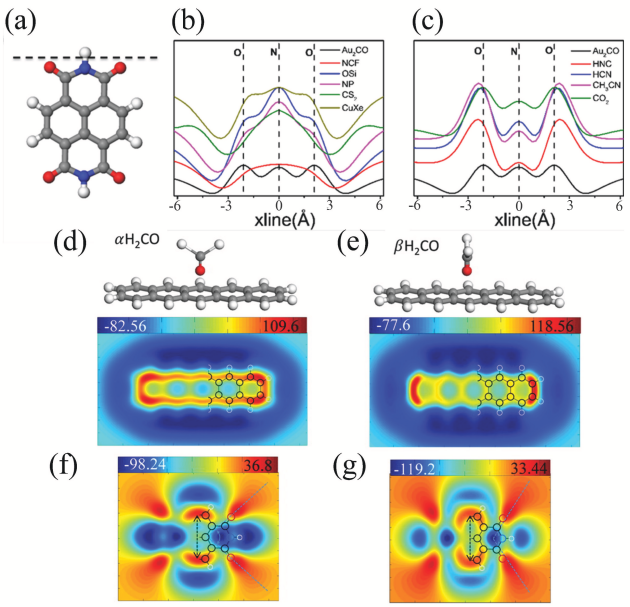

FIG. 12. (a) Ball-and-stick-model of an NTCDI molecule. (b) and (c) Line profile of force acting on various tip molecules. The profile is taken along the black dashed line in (a). Ball-and-stick models of (d) αH_2CO and (e) βH_2CO tip over a pentacene molecule. Here α and β indicate that the direction of hydrogen atoms in H_2CO tip is along and perpendicular to the long axis of the pentacene, respectively. Two-dimensional map of the force acting on the H_2CO tip is also shown below the models. Two-dimensional force map of an NTCDI molecule using (f) αH_2CO and (g) βH_2CO tip. The numbers in the color scale are in pN. Images are reproduced from Ref. [89].

A few studies have attempted to understand the nature of enhancing the AFM resolution by alterations to the tip [83]. A clear difference between Xe and CO is the orbital nature of the molecule. The occupied molecular orbitals of the CO molecule can be characterized as 1σ, 2σ, 1π, and 3σ. Assuming the carbon atom of the CO molecule bonds to the metal tip, the orbital most likely to interact with the specimen is the 2σ orbital. This orbital is localized on the oxygen atom and directed toward the specimen. The 3σ orbital is also directed toward the specimen, but localized on the carbon atom. The other orbitals are not directed at the specimen. Electronic structure computations confirm this analysis for an isolated CO molecule interacting with the specimen [83]. When the molecule interacts with the tip, the orbitals admix and the distinctions between them because ambiguous, although the general picture may still be correct. CO is also special in that it possesses a permanent dipole. This dipole is very sensitive to the CO bond length and depending on

the bond length, can even change sign. Although these features of the CO molecule provide us with some interesting clues, the issue of predicting molecular species for an optimal functionalization of the probe tip remains unresolved.

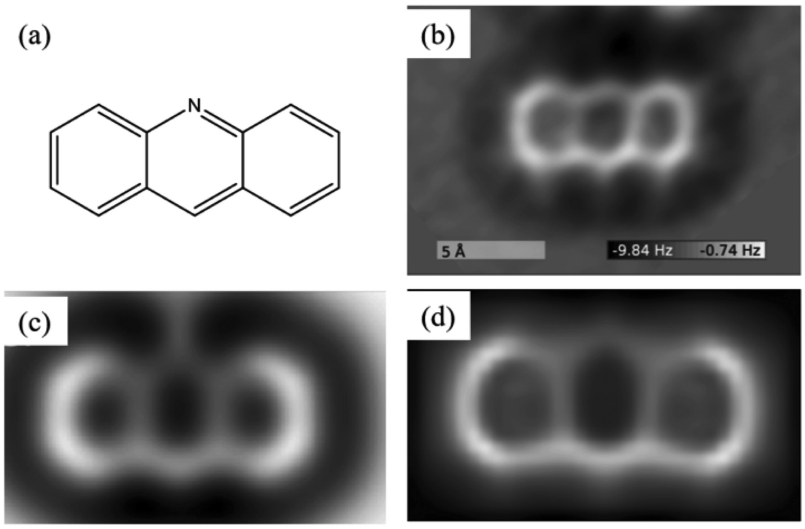

FIG. 13. nc-AFM imaging heteroatom-containing organic compound ACR. (a) Structure of ACR. (b) Experimental nc-AFM image of ACR. (c) and (d) are simulated nc-AFM images of ACR. (c) was obtained with probe particle method, (d) was obtained with full DFT calculation [94]. Figures (b) and (c) are reproduced from Zahl and Zhang [95].

The role of molecular symmetry or orientation is also important for AFM imaging, although the terminal atom is the dominant factor [88, 96]. The symmetry effect is examined by using a H_2CO molecule as shown in the top panels of Figs. 12(d) and 12(e). The two-dimensional maps of the force acting on the tip (the lower panels) show the distortion of the apparent image of the pentacene molecule: stretched along the long and short axis of the molecule in Figs. 12(d) and 12(e), respectively. The force maps on an NTCDI molecule in Figs. 12(f) and 12(g) show a clear distortion caused by the molecular orientation. Interestingly, a significant effect of asymmetry of metallic atoms associated with the tip proper is not found. The stretching effect caused by the molecular symmetry is also confirmed in the simulation of a DBNP molecule [90].

Fig. 13 shows a comparison of simulated nc-AFM image of Acridine (ACR) molecule using (1) probe particle method, which employs interatomic potentials [95], and (2) full DFT calculation [94]. The experimental image [Fig. 13(b)] shows that the N atom in the middle ring can be discriminated as a fainter bright spot comparing with C atom. In Fig. 13(c), the

probe particle method reproduces the faint feature. However, this should not appear, on top of the N atom. The full DFT calculation successfully reproduces the faint feature of N atom as well as the sharp gradient white bar sticking out of each C atom. In this case a quantum treatment is necessary when the chemistry of the functionalized tip is not negligible.

B. Intermolecular bond visualization in AFM

A controversial topic in AFM research is the reported imaging of hydrogen bonds [24–27]. Fig. 14(c) shows an intermolecular feature representing a line between a pair of 8-hydroxyquinoline (8-hq) molecules [24]. This line has been interpreted as the visualization of a hydrogen bonding between hydrogen and nitrogen atoms. On the other hand, a intermolecular bond-like feature was also observed where no bond should exist [97].

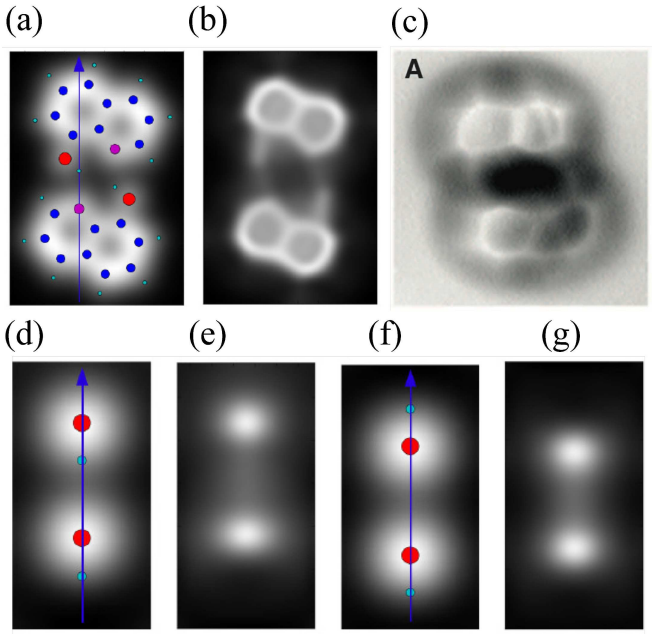

FIG. 14. (a) Simulated AFM image of a pair of 8-hq molecules. Red, blue, skyblue, and magenta circles represent the position of oxygen, carbon, hydrogen, and nitrogen atoms, respectively. (b) Simulated AFM image after applying the tip-relaxation correction. (c) Experimental AFM image of 8-hq molecules. (d) Simulated AFM image of a pair of hydrogen fluoride molecules. The molecules are aligned and have the same orientation. (e) Same as (d) but with tip relaxation correction. (f) Simulated AFM image of a pair of hydrogen fluoride molecules but two molecules have opposite direction to each other. (g) Same as (f) but with tip relaxation. The images are reproduced from Ref. [98] and Ref. [24].

First-principles simulations have been performed to understand the origin of such a inter-

molecular bond feature. Guo *et al.* reported the simulated AFM image of two 8-hq molecules [99]. They confirmed the intermolecular line associated with a hydrogen bond between nitrogen and hydrogen atoms by analyzing the charge density at the intermolecular space. Lee *et al.* also reported the AFM simulation of the same system but in a different relative orientation. Figure 14(a) shows the simulated AFM image of a pair of 8-hq molecules [98]. Here the intermolecular line is not clear but the line becomes clearer when the tip relaxation correction (see Sec. IV B) is applied as shown in Fig.4(b). However, the line connects a nitrogen (magenta circle) and an oxygen atom (red circle), not a hydrogen atom (skyblue circle). The intermolecular line here cannot be associated with the hydrogen bonding, as the line does not appear in between hydrogen and nitrogen atoms. Distinguishing an actual hydrogen bond and the apparent intermolecular line in AFM images is not an easy task.

To further investigate the intermolecular line, Lee *et al.* adopted a model system: a hydrogen fluoride dimer [98]. Two orientations of the HF dimers are prepared as shown in Figs. 14(d) and 14(f). The HF molecules are placed in parallel and anti-parallel directions. The former orientation should induce a hydrogen bond whereas the latter one should not.

Owing to the high electronegativity of the fluorine atom, the charge density is concentrated on the fluorine atom. We note two large circular shaped charge densities before applying the tip relaxation correction as the AFM image. The circle becomes smaller when the correction is applied, and the intermolecular line appears independent of the orientation of HF molecules. This computational experiment confirms that the intermolecular line cannot be necessarily associated with actual bonding as a linear image can result from two concentrated electron densities.

Whether a line appearing in an AFM image is associated with a real chemical bond not can be a complex issue. A bond line has been experimentally observed even within a molecule [a DBTH molecule, see Fig.5(b)]. Extra care is necessary when one attempts to interpret a line in an AFM image with a bond structure. First-principles AFM simulations play an important role in analyzing and understanding such ambiguity in AFM images. Recent experiments utilizing a rigid CuO_x tip report a intermolecular line-like feature, which should not arise from the tip relaxation effect [100, 101]. Some attempts have also been at distinguishing chemical species in the specimen and determining the structure of specimen [48, 102, 103].

VII. COMPUTATIONALLY EFFICIENT FIRST-PRINCIPLES AFM SIMULATION

While fully quantum-mechanical methods can be successfully applied to the AFM simulation of organic molecules with a simplified tip such as a CO molecule, the computational load involved in simulating images can be intense. The situation scales poorly as accurate forces require a highly converged result. These constraints limit such simulations when the size of the target system contains more than a few dozen atoms or when the role of the substrate is important [104].

A system composed of a molecule on a substrate contains a large number of atoms: the tip, the molecule itself and the substrate may contain hundreds of atoms. Also, included is the empty space surrounding the tip/molecule/substrate complex. The computation of tip-sample interaction calculations becomes an enormously difficult job in such a case, especially when one considers that an AFM simulation involves sampling many different configurations. For many systems of interest, simulations are impossible without enormous computational resources. In this section, we outline computationally efficient methods to simulate AFM images based on an approximate density functional theory.

A. Formulation of frozen density embedding theory in AFM simulation

The computational cost of total energy calculations are dramatically reduced if the number of occupied electronic states is decreased. One way to reduce this number is to explicitly treat only the electronic states of the tip. Such an approach works best when the tip-sample interaction is small. For instance, the number of the occupied states in a CO molecule is only five. This means that the number of states used in any AFM simulation can be reduced to five if we could somehow neglect calculations involving the electrons of the specimen.

This approach "reverses" the virtual tip method. The electronic states of the sample are treated approximately whereas the electronic states in the tip are not. One can perform an approximate total-energy calculation by utilizing "frozen density embedding theory" (FDET) [105, 106]. This approach is often used in large biological systems [106] where one wishes to focus on a particular part of the system and avoid the computational load of the entire system.

FDET enables one to divide the charge density of the entire system into two (or more in subsystem DFT configurations[107]) and consider quantum-mechanically only one of the divided charge densities. In the case of AFM simulations, the charge density $\rho^{tot}(\vec{r})$ of the system is divided into two charge densities (an AFM tip and a sample):

$$\rho^{tot}(\vec{r}) = \rho^{t}(\vec{r}) + \rho^{s}(\vec{r}). \tag{18}$$

Here superscripts t and s represent the tip and the sample, respectively. The total energy functional in this formalism is given by

$$\begin{aligned} E_{tot}[\rho^t, \rho^s] = & \int\int \frac{\{\rho^t(\vec{r}) + \rho^s(\vec{r})\}\left\{\rho^t(\vec{r'}) + \rho^s(\vec{r'})\right\}}{2|\vec{r} - \vec{r'}|} d\vec{r} d\vec{r'} \\ & + \int \left\{V^t_{ion}(\vec{r}) + V^s_{ion}(\vec{r})\right\}\left\{\rho^t(\vec{r}) + \rho^s(\vec{r})\right\} d\vec{r} \\ & + T_s[\rho^t] + T_s[\rho^s] + T_s^{nadd}[\rho^t, \rho^s] \\ & + E_{xc}[\rho^t + \rho^s] + E_{ion}, \end{aligned} \tag{19}$$

where V_{ion}, T_s, E_{xc}, and E_{ion} represent the ionic potential, the kinetic energy functional, the exchange-correlation energy functional, and the ion-ion interaction energy, respectively. An FDET total energy calculation is performed with $V^s_{ion}(\vec{r})$ and $n^s(\vec{r})$. The non-additive kinetic energy functional T_s^{nadd} is defined by

$$T_s^{nadd}[\rho^t, \rho^s] = T_s[\rho^t, \rho^s] - T_s[\rho^t] - T_s[\rho^s], \tag{20}$$

is the cross term arising from this frozen approximation.

The exact form of this kinetic energy functional is generally unknown as in the case of the functional for the exchange-correlation energy. An approximate form of the functional must be used to compute the non-additive contribution to the kinetic energy.

Many functional forms have been proposed and discussed in the context of orbital-free density functional theory, where the computation of the kinetic energy is not done by operating the kinetic energy operator acting on wave functions, but by using an analytic form directly. The simplest form of such an approximation is Thomas-Fermi kinetic energy func-

tional:

$$T_s^{TF}[\rho] = C_{TF} \int \rho^{5/3} d\vec{r}. \tag{21}$$

Here the parameter C_{TF} is equal to 2.871. This approximation corresponds to the LDA in exchange-correlation functional [55]. The simplicity of the Thomas-Fermi functional is computationally beneficial, but this form fails to bind atoms.

The inclusion of the gradient of density can improve the results in a similar fashion to the case of exchange-correlation functional. For example, the Lembraki-Chermette gradient-corrected functional is one of the widely used such gradient-corrected functional [108]. The kinetic energy functional illustrated in this review also includes charge density gradient, which is developed by Tran and Wesolowski [109]:

$$T_s^{TW}[\rho] = \frac{3}{10}(3\pi^2)^{2/3} \int \rho^{5/3} F_t\left(s(\vec{r})\right) d\vec{r}. \tag{22}$$

Here

$$F_t(s) = 1 + \kappa - \frac{\kappa}{1 + \frac{\mu}{\kappa} s^2} \tag{23}$$

is an enhancement factor which is a function of reduced density gradient $s(\vec{r}) = |\nabla\rho|/2\rho k_F$ where $k_F = (3\pi^2\rho)^{1/3}$. Here the parameters $\mu = 0.2309$ and $\kappa = 0.8589$ are chosen so that this function can reproduce the kinetic energy of rare-gas atoms. This functional form is exactly the same as the Perdew-Burke-Ernzerhof exchange-correlation functional [110], although these parameters differ from the original values.

A Schrödinger-like equation in the FDET for a set of eigenvalues and wave functions of tip electronic states ($\{\epsilon_i^t, \psi_i^t(\vec{r})\}$) is

$$\left[\frac{-\nabla^2}{2} + V_{eff}^t(\vec{r}) + V_{emb}(\vec{r})\right] \psi_i^t(\vec{r}) = \epsilon_i^t \psi_i^t(\vec{r}). \tag{24}$$

The potential term here is divided into two: the effective Kohn-Sham potential of the tip

$$V_{eff}^t(\vec{r}) = \int \frac{\rho^t(\vec{r'})}{|\vec{r} - \vec{r'}|} d\vec{r'} + V_{ion}^t(\vec{r}) + \left.\frac{\delta E_{xc}[\rho]}{\delta\rho}\right|_{\rho=\rho^t}, \tag{25}$$

and an embedded potential

$$V_{emb}(\vec{r}) = \int \frac{\rho^s(\vec{r'})}{|\vec{r} - \vec{r'}|} d\vec{r'} + V^s_{ion}(\vec{r}) + \left.\frac{\delta E_{xc}[\rho]}{\delta \rho}\right|_{\rho=\rho^{tot}} - \left.\frac{\delta E_{xc}[\rho]}{\delta \rho}\right|_{\rho=\rho^{t}} + \left.\frac{\delta T_s[\rho]}{\delta \rho}\right|_{\rho=\rho^{tot}} - \left.\frac{\delta T_s[\rho]}{\delta \rho}\right|_{\rho=\rho^{t}}, \quad (26)$$

arising from the frozen charge density of the sample. Equation 24 is solved self-consistently in the same way as normal DFT total energy calculations.

In a practical AFM simulation with the FDET, first a full DFT total-energy calculation must be done for a sample to obtain the charge density of the sample. This charge density is stored for the following AFM simulation. The AFM simulation is performed by computing total energies on a uniform grid over the sample charge density in the same way as the full DFT AFM simulation. The FDET-based AFM simulation algorithm has been implemented in a real-space pseudopotential DFT code [53, 54, 61], and applied to several systems [64, 90].

B. Validation and application

We introduce the case of a CO molecule tip over a benzene molecule to evaluate the performance of the FDET to AFM simulations [64]. Figure 15 shows the computed interaction energy between CO tip and benzene sample as a function of tip-sample distance for three different sites in a benzene molecule. The equilibrium tip-sample distance is underestimated by 0.3 to 0.4 Å in FDET simulations. In addition, the equilibrium interaction energies are also underestimated by 10 to 20 meV.

There discrepancies arise from the approximate nature of the FDET method. Fortunately the errors are not large and when the relative values among three sites are considered, the error can be smaller. The energy and distance difference between C and h sites are -5 meV and 0.32 Å, respectively in the DFT case whereas those in the FDET case are -6 meV and 0.21 Å. The frequency shift as function of tip-sample distance is also expected to be reproduced by using the FDET method. Consequently, the FDET-based method should qualitatively reproduce DFT-simulated AFM images even though the agreement between total energy curves is not perfect.

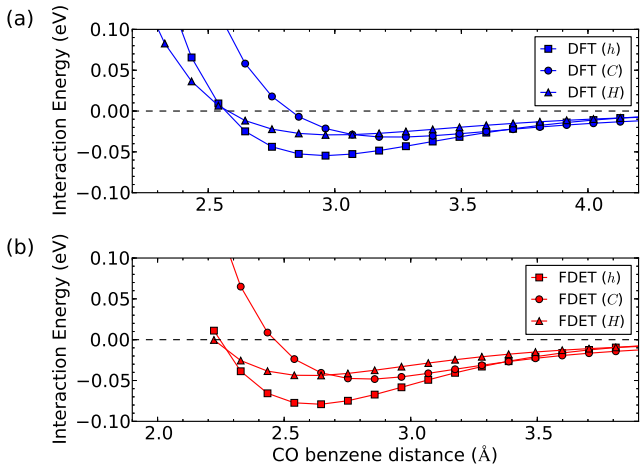

FIG. 15. Tip-sample interaction energy as a function of distance computed by using (a) Full DFT and (b) FDET. Squares, circles, and triangles represent that a CO molecule is above hollow (h), carbon (C), and hydrogen (H) sites of a benzene molecule, respectively. This figure is reproduced from Ref. [64] by permission granted from ACS publication.

The actual performance of the FDET method on AFM simulation can be tested against a pentacene molecule with a CO molecule as a tip. Figures 16(a) and 16(b) show the simulated AFM image of pentacene based on full DFT and FDET total energy calculations, respectively. The simulated tip heights are 3.39 Å and 3.07 Å for DFT and FDET, respectively so that the underestimation of equilibrium distance in the FDET is incorporated. The characteristic bright edge and resolved inner chemical bond in the full DFT simulation is well reproduced in the FDET simulation. On the other hand, the simulated image with the virtual tip method cannot resolve the inner bond of the molecule. The FDET is clearly more accurate than the virtual tip method. This result also confirms that an explicit model of a tip is important for simulations of a CO-functionalized AFM.

Both DFT- and FDET-simulated images capture characteristics of the experimental AFM image of pentacene [Fig. 16(e)]. However, the agreement is not perfect; the covalent bonds are thin and the imaged molecule shows asymmetry between upper and lower half in the experimental image.

The AFM experiment was performed on a sample on a Cu(111) substrate while the simulation above assumes completely flat molecule. When the molecule is placed on Cu(111), first-principles simulation shows that the molecule is tilted along the short side. The substrate also lifts up the edge hydrogen atoms. The substrate effect induces the asymmetry of the imaged pentacene (lower half is brighter) and enhanced brightness of the edge.

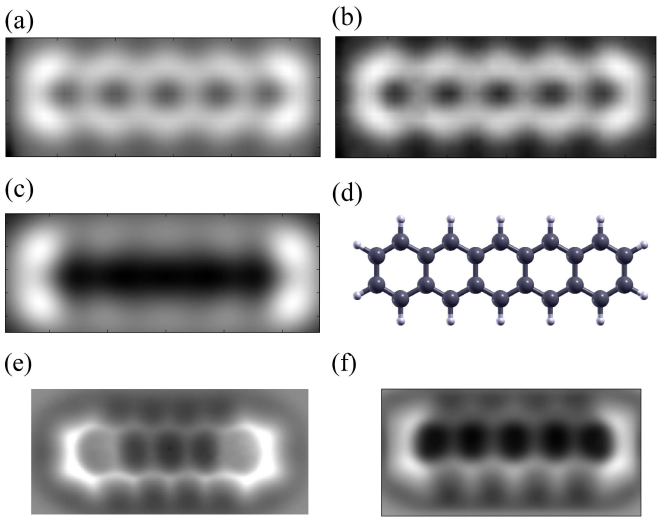

FIG. 16. Simulated AFM images of pentacene with (a) full DFT, (b) FDET, and (c) virtual tip methods. (d) Ball and stick model of pentacene. Here Gray and white spheres represent carbon and hydrogen atoms, respectively.(e) Experimental AFM image. The pentacene molecule was placed on a Cu(111) substrate. (f) Simulated AFM image with FDET. The molecular structure is first relaxed on a Cu(111) substrate and simulation is done in a confined sphere with the substrate removed. A tip relaxation correction [67] is applied by using an estimated lateral spring constant k of 0.24 N/m [111]. The tip heights for the AFM simulations are 3.39 Å for (a) and (c), and 3.07 Å for (b) and (f). Figures (a), (b), (c) were reproduced from Ref. [64], (e) is from Ref. [74].

The tip relaxation effect can be taken into account as well and it makes the bonds thinner. Figure 16(f) shows a highly improved simulated image with the substrate and tip relaxation effect [94]. After considering all these factors, the simulation performance becomes dramatically improved.

The simulated images agree well with experiment even without considering these factors when a sample has relatively flat surfaces and high symmetry. An organic molecule such as hexabenzocoronene has a highly symmetric structure as shown in the FDET-simulated image Fig. 17(a). The simulated image agrees with the experimental image shown in Fig. 17(b). Similarly, an inorganic monolayer Cu_2N on Cu(100) can be simulated without tilting correction. The simulated image of Cu_2N monolayer is shown in Fig. 17(c). The brightest and darkest spots appear at nitrogen and copper sites, respectively in both simulated and experimental [Fig. 17(d)] images. This example also shows that the FDET method can be extended to the combination of an inorganic surface and a CO tip.

The computational saving of the FDET method is considerable in systems with a large number of electrons. A molecule such as hexabenzocoronene molecule ($C_{42}H_{18}$) has 186

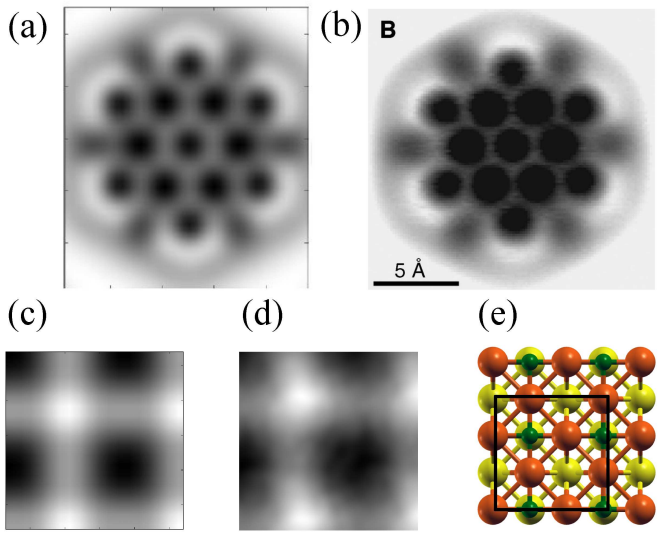

FIG. 17. (a) Simulated AFM image of a hexabenzocoronene molecule [112]. The simulation is performed without tip relaxation correction. (b) Experimental AFM image of the molecule. (c) Simulated and (d) experimental AFM images of a Cu_2N monolayer on a Cu(100) substrate. The simulation is done with a tip height of 2.75 Å and without tip relaxation correction. (e) Ball and stick model of a Cu_2N monolayer on Cu(100). Green spheres show nitrogen atoms. Orange and yellow spheres represent copper atoms at and underneath the surface, respectively. The figure shows the periodic cell while the black squared region shows the imaged region. Figure (b) is taken from Ref. [15]. Figures (c) and (e) are reproduced from Ref. [64] with a permission granted by ACS publication. (d) is from Ref. [113].

electrons and 93 occupied electronic states. Save for an initial computation, these electronic states can be completely neglected in the FDET simulations. Only the five occupied states of a CO molecule need be updated quantum mechanically. This number reduction is considerable since the computational cost of total energy calculation scales superlinearly with the number of desired states.

Another example of a "large" system is the Cu_2N monolayer on a Cu(100) substrate. Such a surface system is typically modeled by using finite bulk layers in DFT simulations. As a result, here the number of the electrons in the system is 656 and the number of the occupied states are 328. In addition, a $\vec{k}$ point sampling in the Brillouin zone is generally required for simulations of such a periodic surface. The number of $\vec{k}$ points required is 20, thus in total 6560 states must be considered. However, such a $\vec{k}$ point sampling can be neglected [114] when we consider only the tip electronic states. Therefore, the electronic states to be computed is again only five. The reduction of the computational load here is more considerable than the previous hexabenzocoronene case. The AFM simulation of such

a large system is possible, but not practical, without using the FDET-based AFM simulation method.

The FDET-based AFM simulation is not suitable for the AFM simulations with a reactive tip such as copper. In fact, Lee *et al.*, show that the FDET-based AFM simulation of the Cu_2N monolayer with a Cu tip cannot reproduce the experimental results [65, 113]. The amplitude of the force acting on a tip is typically around a few nN in such a reactive tip whereas the amplitude is expected to be around a hundred pN in FDET. Such a strong interaction is beyond the assumption of the FDET that the tip electronic states are not affected much. In such a highly reactive tip case, the FDET fails to reproduce the tip-sample interaction computed by using full DFT method.

VIII. CONCLUSIONS

We illustrated several approaches to simulating non-contact atomic force microscopy images. A summary of the approaches introduced with some brief comments is given in Table I.

The simplest and most computationally tractable approach is to approximate forces between the probe tip and the specimen with interatomic potentials. Such an approach works well in assessing structural models for ionic materials, but fails to include many body potentials as might be appropriate for covalent materials and does not include chemical forces that result as hybridization changes, save in an *ad hoc* fashion. Moreover, the construction of an interatomic potential often involves the transcription of quantum forces to classical ones. There is no direct formulation for the construction of classical forces from quantum forces, and the use of empirical potentials can be problematic. An example of this situation is illustrated in Fig. 11. Two images are shown. One with a classical probe tip and one with a CO tip. The difference in the resolution is striking. The model with the CO probe tip distinctly reflects a subatomic resolution of the covalent bond. Without a distinction between classical and quantum forces, it would be hard to understand such as result. The corresponding image based solely on classical potentials is problematic at best. Likewise, analyzing hydrogen bonds as in Fig. 14 through the use of classical potentials is outside the scope of such descriptions.

A method capable of a "quick screening" of structural models centers on the use of a "virtual tip." In this approach, the tip is replaced by a classical probe, which is characterized by

Method	Comments
Interatomic potentials	Easy to implement and computationally efficient. May not accurately reproduce quantum related forces.
Virtual tip	Avoids structure of tip. Treats tip as classical object. Computationally simple. Lacks chemical description of functionalized tip.
Frozen density	Treats the tip within quantum description. Avoids explicit computation of the specimen, save to compute fixed charge density. Significant reduction of computational load. Limited to weakly interacting systems.
Quantum computations	Most accurate method. New eigensolver algorithms greatly reduce computational load. Remains computationally intensive for large systems.

TABLE I. Approaches to simulating non-contact atomic force microscopy images with comments.

a constant polarizability. The virtual tip responds to the electrostatic field generated by the specimen. The computational load consists of computing a fixed field of the specimen with quantum based methods and can be orders of magnitude faster than a full quantum computation. This method includes explicit electrostatic contributions and correctly distinguishes atomic force microscopy images that might be attributed to chemical bonds, but are not. The method cannot describe chemically active tips. For example, the virtual tip method best describes a probe functionalized with an inert gas such as a Xe. The method cannot account for the enhanced resolution of tip functionalized with CO. However, the method can distinguish images where AFM might otherwise lead to incorrect interpretations.

An intriguing approach is to "reverse" the virtual tip approach by fully treating the probe tip by a quantum computation and determining the changes in forces by moving the tip within a fixed electrostatic field of the specimen. This configuration merits strong consideration as a future technique as the forces in a non-contact mode are weak with the tip unlikely to alter the electrostatic field of the specimen. While methods based on complete separation of the tip electron density from the specimen electron density fail to match the measured images, the interaction of the specimen density with the tip density can be included in an approximate fashion. The specimen density can be fixed and a density functional formalism for non-additive terms can be utilized. In particular, it is possible to use formalisms developed for weakly interacting systems such as density embedding theory. This approach works well and dramatically lowers the computational costs as only the states

associated with the probe tip must be explicitly included. The method is limited if the probe and specimen interact strongly. However, it is a solid way to proceed as quantum forces can be well defined. Extensions of this method are clearly promising.

The most accurate approach is where the tip, specimen and substrate are included explicitly in a quantum computation. Reliable forces based on such quantum simulations can be essential for an accurate interpretation of AFM images. Unquestionably, the use of quantum forces is the most promising pathway for simulating AFM images. The formalism is applicable to a wide variety of materials and best approximates many body interactions without the use of *ad hoc* parameters. Moreover, advances in electronic structure theory has allowed systems of unprecedented size to be addressed [59, 60, 62]. We expect such advances to continue along with the development of new hardware. For example, current eigensolvers can be improved by the implementation of additional layer of parallelism by solving the Kohn-Sham eigenvalue problem for a given energy window [62]. This area of study offers the possibility of accurate AFM simulated images for systems that are currently computationally limited.

ACKNOWLEDGEMENTS

We acknowledge support from the Welch Foundation under grant F-1837 and from the U.S. Department of Energy (DOE) under DOE/DE-FG02-06ER46286. Computational resources were provided by the National Energy Research Scientific Computing (NERSC) and the Texas Advanced Computing Center (TACC).

[1] K. Kostiropoulos W. Krätschmer, L.D. Lamb and D. R. Hoffman, "Solid C_{60}: A new form of carbon," Nature **347**, 354 (1990).

[2] M.M. Kappes S. Liu, Y.-J. Lu and J.A. Ibers, "The structure of the C_{60} molecule: X-ray crystal sructure dtermination of a twin at 110 K." Science **254**, 408 (1991).

[3] Editorial, "25 years of C_{60}," Nat. Nanotechnol. **5**, 691 (2010).

[4] F. J. Giessibl, "Advances in atomic force microscopy," Rev. Mod. Phys. **75**, 949 (2003).

[5] C. Barth, A. S. Foster, C. R. Henry, and A. L. Shluger, "Recent trends in surface characterization and chemistry with high-resolution scanning force methods," Adv. Mater. **23**, 477 (2011).

[6] P. Jelinek, "High resoultion SPM imaging of organic molecules with functionalized tips," J. Phys.: Condensed Matter **29**, 343002 (2017).

[7] A.S. Foster W.A. Hofer and A.L. Shluger, "Theories of scanning probe microscopies at the atomic scale," Rev. Mod. Phys. **75**, 1287 (2003).

[8] G. Binnig, H. Rohrer, Ch. Gerber, and E. Weibel, "Tunneling through a controllable vacuum gap," Appl. Phys. Lett. **40**, 178 (1982).

[9] G. Binnig, H. Rohrer, Ch. Gerber, and E. Weibel, "Surface studies by scanning tunneling microscopy," Phys. Rev. Lett. **49**, 57 (1982).

[10] R. García and R. Pérez, "Dynamic atomic force microscopy methods," Surf. Sci. Rep. **47**, 197 (2002).

[11] F. Giessibl, "The qPlus sensor, a powerful core for the atomic force microscope," Rev. Sci. Instru. **90**, 011101 (2019).

[12] G. Binnig, C. F. Quate and Ch. Gerber, "Atomic force microscope," Phys. Rev. Lett. **56**, 930 (1986).

[13] T. R. Albrecht, P. Grütter, D. Horne, and D. Ru, "Frequency modulation detection using high-q cantilevers for enhanced force microscope sensitivity," J. Appl. Phys **69**, 668 (1991).

[14] F. J. Giessibl, "Atomic resolution of the silicon (111)-(7x7) surface by atomic force microscopy," Science **267**, 678 (1995).

[15] L. Gross, F. Mohn, N. Moll, B. Schuler, A. Criado, E. Guitián, D. Peña, A.Gourdon, and G.Meyer, "Bond-order discrimination by atomic force microscopy," Science **337**, 1326 (2012).

[16] M. Neu, N. Moll, L. Gross, G. Meyer, F. J. Giessibl, and J. Repp, "Image correction for atomic force microscopy images with functionalized tips," Phys. Rev. B **89**, 205407 (2014).

[17] H. Labidi, M. Koleini, T. Huff, M. Salomons, M. Cloutier, J. Pitters, and R. A. Wolkow, "Indications of chemical bond contrast in afm images of a hydrogen-terminated silicon surface," Nat. Comm. **8**, 14222 (2017).

[18] M. Ellner, P. Pou, and R. Pérez, "Molecular identification, bond order discrimination, and apparent intermolecular features in atomic force microscopy studied with a charge density based method," ACS Nano **13**, 786 (2019).

[19] L. Gross, F. Mohn, N. Moll, G. Meyer, R. Ebel, W.M. Abdel-Mageed, and M. Jaspars, "Organic structure determination using atomic-resolution scanning probe microscopy," Nat. Chem. **2**, 821 (2010).

[20] R. Pérez, "Discriminating chemical bonds," Science **337**, 1305 (2012).

[21] B. Schuler, W. Liu, A. Tkatchenko, N. Moll, G. Meyer, A. Mistry, D. Fox, and L. Gross, "Adsorption geometry determination of single molecules by atomic force microscopy," Phys. Rev. Lett. **111**, 106103 (2013).

[22] A. Mistry, B. Moreton, B. Schuler, F. Mohn, G. Meyer, L. Gross, A. Williams, P. Scott, G. Costantini, and D. J. Fox, "The synthesis and STM / AFM imaging of Olympicene' benzo[cd]pyrenes," Chem. Eur. J **21**, 2011 (2015).

[23] B. Schuler, G. Meyer, D. Peña, O. C. Mullins and L. Gross, "Unraveling the molecular structures of asphaltenes by atomic force microscopy," J. Am. Chem. Soc. **137**, 9870 (2015).

[24] J. Zhang, P. Chen, B.i Yuan, W. Ji, Z.i Cheng, and X. Qiu, "Real-space identification of intermolecular bonding with atomic force microscopy," Science **342**, 611 (2013).

[25] C.-L. Chiang, C. Xu, Z. Han, and W. Ho, "Real-space imaging of molecular structure and chemical bonding by single-molecule inelastic tunneling probe," Science **344**, 885 (2014).

[26] A. M. Sweetman, S. P. Jarvis, H. Sang, I. Lekkas, P. Rahe, Yu Wang, J. Wang, N. R. Champness, L. Kantorovich, and P. Moriarty, "Mapping the force field of a hydrogen-bonded assembly," Nature Commun. **5**, 3931 (2014).

[27] A. Shiotari and Y. Sugimoto, "Ultrahigh-resolution imaging of water networks by atomic force microscopy," Nature Commun. **8**, 14313 (2017).

[28] M. Emmrich, F. Huber, F. Pielmeier, J. Welker, T. Hofmann, M. Schneiderbauer, D. Meuer, S. Polesya, S. Mankovsky, Diemo Kodderitzsch, H. Ebert, and F. J. Giessibl, "Subatomic

resolution force microscopy reveals internal structure and adsorption sites of small iron clusters," Science **348**, 308 (2015).

[29] A. Bogner, P.-H. Jouneau, G. Thollet, D. Basset, and C. Gauthier, "A history of scanning electron microscopy developments: Towards "wet-STEM" imaging," Micron **38**, 390 (2007).

[30] F. J. Giessibl, "Forces and frequency shifts in atomic-resolution dynamic-force microscopy," Phys. Rev. B **56**, 16010 (1997).

[31] F. J. Giessibl, "A direct method to calculate tip–sample forces from frequency shifts in frequency-modulation atomic force microscopy," Appl. Phys. Lett. **78**, 123 (2001).

[32] J. Tersoff and D. R. Hamann, "Theory of the scanning tunneling microscope," Phys. Rev. B **31**, 805 (1985).

[33] Y. G. Ding, C. T. Chan and K. M. Ho, "Structure of the $(\sqrt{3} \times \sqrt{3})$R30°Ag/Si(111) surface from first principles calcuilations," Phys. Rev. Lett. **67**, 1454 (1991).

[34] N. Pavliček, C. HerranzLancho, B. Fleury, M. Neu, J. Niedenführ, M. Ruben, and J. Repp, "Highresolution scanning tunneling and atomic force microscopy of stereochemically resolved dibenzo [a, h] thianthrene molecules," phys. stat. solidi (b) **250**, 2424 (2013).

[35] N. Moll, L. Gross, F. Mohn, A. Curioni, and G. Meyer, "The mechanisms underlying the enhanced resolution of atomic force microscopy with functionalized tips," New J. Phys. **12**, 125020 (2010).

[36] N. Moll, L. Gross, F. Mohn, A. Curioni, and G. Meyer, "A simple model of molecular imaging with noncontact atomic force microscopy," New J. Phys. **14**, 083023 (2012).

[37] S. Morita, "Atomically resolved force microscopy," J. Vac. Sci. Tech. A **31**, 050802 (2013).

[38] S. Kawai F. Xu L. Peng A. Orita J. Otera A. Curioni M. Neu J. Repp G. Meyer N. Moll, B. Schuler and L. Gross, "Image distortions of a partially fluorinated hydrocarbon molecule in atomic force microscopy with carbon monoxide terminated tips," Nano Lett. **14**, 6127 (2014).

[39] P. Hapala D. Cao R. Ma B. Cheng L. Xu M. Ondráček P. Jelínek E. Wang J. Peng, J. Guo and Y. Jiang, "Weakly perturbative imaging of interfacial water with submolecular resolution by atomic force microscopy," Nature Commun. **9**, 122 (2018).

[40] S. Maskey P. T. Mikulski M. T. Knippenberg J. A. Harrison, J. D. Schall and B. H. Morrow, "Review of force fields and intermolecular potentials used in atomistic computational materials research," Appl. Phys. Rev. **5**, 031104 (2018).

[41] J. Tracey, F. F. Canova, O. Keisanen, D. Z. Gao, P. Spijker, B. Reischl, and A. S. Foster, "Flexible and modular virtual scanning probe microscope," Comp. Phys. Commun. **196**, 429 (2015).

[42] F. Schulz, J. Ritala, O. Krejci, A. P. Seitsonen, A. S. Foster, and P. Liljeroth, "Elemental identification by combining atomic force microscopy and kelvin probe force microscopy," ACS Nano **12**, 5274 (2018).

[43] M. Guggisberg, M. Bammerlin, Ch. Loppacher, O. Pfeiffer, A. Abdurixit, V. Barwich, R. Bennewitz, A. Baratof, E. Meyer and H.J. Güntherodt, "Separation of interactions by noncontact force microscopy," Phys. Rev. B **61**, 11151 (2000).

[44] K. Ruschmeier, A. Schirmeisen, and R. Hoffmann, "Atomic-scale force-vector fields," Phys. Rev. Lett. **101**, 156102 (2008).

[45] A. I. Livshits, A. L. Shluger, A. L. Rohl, and A. S. Foster, "Model of noncontact scanning force microscopy on ionic surfaces," Phys. Rev. B **59**, 2436 (1999).

[46] A. S. Foster, C. Barth, A. L. Shluger, and M. Reichling, "Unambiguous interpretation of atomically resolved force microscopy images of an insulator," Phys. Rev. Lett. **86**, 2373 (2001).

[47] C. Barth, A. S. Foster, M. Reichling, and A. L. Shluger, "Contrast formation in atomic resolution scanning force microscopy on CaF_2(111): Experiment and theory," J. Phys.: Condens. Matter **13**, 2061 (2001).

[48] G. Teobaldi, K. Lammle, T. Trevethan, M. Watkins, A. Schwarz, R. Wiesendanger, and A. L. Shluger, "Chemical resolution at ionic crystal surfaces using dynamic atomic force microscopy with metallic tips," Phys. Rev. Lett. **106**, 216102 (2011).

[49] D. Z. Gao, J. Grenz, M. B. Watkins, F. F. Canova, A. Schwarz, R. Wiesendanger, and A. L. Shluger, "Using metallic noncontact atomic force microscope tips for imaging insulators and polar molecules: Tip characterization and imaging mechanisms," ACS Nano **8**, 5339 (2014).

[50] S. Sanna, C. Dues and W.G. Schmidt, "Modeling atomic microscopy at $LiNbO_3$ surfaces from first principles," Comput. Mater. Sci. **103**, 145 (2015).

[51] M.L. Cohen, "Pseudopotentials and total energy calculations," Phys. Scr. **T1**, 5 (1982).

[52] N. Troullier and J. L. Martins, "Efficient pseudopotentials for plane-wave calculations," Phys. Rev. B **43**, 1993–2006 (1991).

[53] J. R. Chelikowsky, "The pseudopotential-density functional method (PDFM) applied to nanostructures," J. Phys. D **33**, R33 (2000).

[54] J.R. Chelikowsky, N. Troullier, and Y. Saad, "Finite-difference-pseudopotential method: electronic structure calculations without a basis," Phys. Rev. Lett. **72**, 1240 (1994).

[55] W. Kohn and L. J. Sham, "Self-Consistent Equations Including Exchange and Correlation Effects," Phys. Rev. **140**, A1133 (1965).

[56] P. Hohenberg and W. Kohn, "Inhomogeneous Electron Gas," Phys. Rev. **136**, B864–B871 (1964).

[57] D. M. Ceperley and B. J. Alder, "Ground State of the Electron Gas by a Stochastic Method," Phys. Rev. Lett. **45**, 566–569 (1980).

[58] T.L. Beck, "Real-space mecs techiniques in density functional theory," Rev. Mod. Phys. **72**, 1041 (2000).

[59] Y. Saad, J.R. Chelikowsky and S. Shontz, "Numerical methods for electronic structure calculations of materials," SIAM Review **52**, 3 (2010).

[60] Y. Zhou, Y. Saad, M.L. Tiago and J.R. Cheikowsky, "Parallel self-consistent-field calculations via Chebyshev-filtered subspace acceleration," Phys. Rev. E **74**, 066704 (2006).

[61] A. Natan, A. Benjamini, D. Naveh, L. Kronik, M. L. Tiago, S. P. Beckman, and J. R. Chelikowsky, "Real-space pseudopotential method for first principles calculations of general periodic and partially periodic systems," Phys. Rev. B **78**, 075109 (2008).

[62] G. Schofield, J.R. Chelikowsky and Y. Saad, "A spectrum slicing method for the Kohn-Sham problem," Comp. Phys. Commun. **183**, 497 (2012).

[63] L. Frediani and D. Sundholm, "Real-space numerical grid methods in quantum chemistr," Phys. Chem. and Chem. Phys. **17**, 31357 (2015).

[64] Y. Sakai, A.J. Lee, and J.R. Chelikowsky, "First-principles atomic force microscopy image simulations with density embedding theory," Nano Lett. **16**, 3242 (2016).

[65] A.J. Lee, Y. Sakai, and J.R. Chelikowsky, "Simulating contrast inversion in atomic force microscopy imaging with real-space pseudopotentials," Phys. Rev. B **95**, 081401 (2017).

[66] P. Hapala, G. Kichin, C. Wagner, S.F. Tautz, R. Temirov, and J. Pavel, "Mechanism of high-resolution STM/AFM imaging with functionalized tips," Phys. Rev. B **90**, 085421 (2014).

[67] C.-S. Guo, M. A. Van Hove, X. Ren, and Y. Zhao, "High-resolution model for noncontact atomic force microscopy with a flexible molecule on the tip apex," J. Phys. Chem. C **119**,

1483 (2015).

[68] B. Bat-Uul, S. Fujii, T. Shiokawa, T. Ohzono and M. Fujihira, "Molecular dynamics simulation of non-contact atomic force microscopy of self-assembled monolayers on Au(111)," Nanotechnology **15**, 710 (2004).

[69] X. Hu, P. Egberts, Y. Dong and A. Martini, "Molecular dynamics simulation of amplitude modulation atomic force microscopy," Nanotechnology **26**, 235705 (2015).

[70] T.-L Chan, C. Z. Wang, K. M. Ho, and J.R. Chelikowsky, "Efficient first-principles simulation of noncontact atomic force microscopy for structural analysis," Phys. Rev. Lett. **102**, 176101 (2009).

[71] M. Katayama, R. S. Williams, M. Kato, E. Nomura, and M. Aono, "Structure analysis of the Si(111) $\sqrt{3} \times \sqrt{3}$ $R30^0$- Ag surface," Phys. Rev. Lett. **66**, 2762 (1991).

[72] T. Minobe, T. Uchihashi, T. Tsukamoto, S. Orisaka, Y. Sugawara, and S. Morita, "Distance dependence of noncontact-AFM image contrast on Si(111)3×3–Ag structure," Appl. Surf. Sci. **140**, 298 (1999).

[73] N. Sasaki, H. Aizawa, and M. Tsukada, "Theoretical simulation of noncontact AFM images of Si(111) $\sqrt{3}$ $\times\sqrt{3}$ - Ag surface based on Fourier expansion method," Appl. Surf. Sci. **157**, 367 (2000).

[74] L. Gross, F. Mohn, N. Moll, P. Liljeroth, and G. Meyer, "The chemical structure of molecule resolved by atomic force microscopy," Science **325**, 1110 (2009).

[75] M. Ellner, P. Pou, and R. Pérez, "Atomic force microscopy contrast with CO functionalized tips in hydrogen-bonded molecular layers: Does the real tip charge distribution play a role?" Phys. Rev. B **96**, 075418 (2017).

[76] M. Ellner, N. Pavliček, P. Pou, B. Schuler, N. Moll, G. Meyer, L. Gross, and R. Pérez, "The electric field of CO tips and its relevance for atomic force microscopy," Nano Lett. **16**, 1974 (2016).

[77] N. Pavliček, B. Schuler, S. Collazos, N. Moll, D. Pérez, E. Guitián, G. Meyer, D. Peña, and L. Gross, "On-surface generation and imaging of arynes by atomic force microscopy," Nat. Chem. **7**, 623 (2015).

[78] Dimas G. de Oteyza, Patrick Gorman, Y.-C. Chen, Sebastian Wickenburg, Alexander Riss, Duncan J. Mowbray, Grisha Etkin, Zahra Pedramrazi, H.-Z. Tsai, Angel Rubio, Michael F. Crommie, and Felix R. Fischer, "Direct imaging of covalent bond structure in single-molecule

chemical reactions," Science **340**, 1434–1437 (2013).

[79] J. van der Lit, F. Di Cicco, P. Hapala, P. Jelinek, and I. Swart , "Submolecular resolution imaging of molecules by atomic force microscopy: The influence of the electrostatic force," Phys. Rev. Lett. **116**, 096102 (2016).

[80] J. Welker and F. J. Giessibl, "Revealing the angular symmetry of chemical bonds by atomic force microscopy," Science **336**, 444 (2014).

[81] J. Welker, A. J. Weymouth, and F. J. Giessibl, "The influence of chemical bonding configuration on atomic identification by force spectroscopy," ACS Nano **7**, 7377 (2013).

[82] T. Hofmann, F. Pielmeier, and F. J. Giessibl, "Chemical and crystallographic characterization of the tip apex in scanning probe microscopy," Phys. Rev. Lett. **112**, 066101 (2015).

[83] M. Kim and J.R. Chelikowsky, "CO tip functionalization in subatomic resolution atomic force microscopy," Appl. Phys. Lett. **107**, 163109 (2015).

[84] F. Mohn, B. Schuler, L. Gross, and G. Meyer, "Different tips for high-resolution atomic force microscopy and scanning tunneling microscopy of single molecules," Appl. Phys. Lett. **102**, 073109 (2013).

[85] P. Schaffhauser and S. Kümmel, "Simulating atomic force microscope images with density functional theory: The role of nonclassical contributions to the force," Phys. Rev. B **94**, 035426 (2016).

[86] M. Ashino, A. Schwarz, H. Hölscher, U. D. Schwarz, and R. Wiesendanger, "Interpretation of the atomic scale contrast obtained on graphite and single-walled carbon nanotubes in the dynamic mode of atomic force microscopy," Nanotechnology **16**, S134 (2005).

[87] A. Sánchez-Grande, B. de la Torre, J. Santos, B. Cirera, K. Lauwaet, T. Chutora, S. Edalatmanesh, P. Mutombo, J. Rosen, R. Zbořil, R. Miranda, J. Björk, P. Jelínek, N. Martín and D. Écija, "On surface synthesis of ethynylene-bridged anthracene polymers," Angew. Chem. Int. Ed. **58**, 6559 (2019).

[88] C.-S. Guo, M.A. Van Hove, R.-Q. Zhang, and C. Minot, "Prospects for resolving chemical structure by atomic force microscopy: A first-principles study," Langmuir **26**, 16271 (2010).

[89] X. Xin, L.-Y. Gan, M.A. Van Hove, X. Ren, H. Wang, C.-S. Guo, and Y Zhao, "Exploring molecules beyond CO as tip functionalizations in high-resolution noncontact atomic force microscopy: A first principles approach," ACS Omega **1**, 1004 (2016).

[90] D. Fan, Y. Sakai, and J. R. Chelikowsky, "Real-space pseudopotential calculations for simulating noncontact atomic force microscopy images," J. Vac. Sci. Tech. B **36**, 04H102 (2018).

[91] A. Shiotari and Y. Sugimoto, "Ultrahigh-resolution imaging of water network by atomic force microscopy," nat. comm. **8**, 14313 (2017)." Nat. Commun. **8**, 14313 (2017).

[92] A. S. Foster, A. L. Shluger, and R. M. Nieminen, "Realistic model tips in simulations of nc-AFM," Nanotechnology **15**, S60 (2004).

[93] T. Chutora, B. de la Torre, P. Mutombo, J. Hellerstedt, J. Kopeček, P. Jelínek and M. Švec, "Nitrous oxide as an effective AFM tip functionalization: a comparative study," Belistein J. Nanotechnol. **10**, 315 (2019).

[94] D. Fan, Y. Sakai, A.J. Lee, and J. R. Chelikowsky, (to be published).

[95] P. Zahl and Y. Zhang, "Guide for atomic force microscopy image analysis to discriminate heteroatoms in aromatic molecules," Energy Fuels **33**, 6 (2019).

[96] V. Caciuc and H. Hölscher, "Ab initio simlation of atomic-scale imaging in noncontact atomic force microscopy," Nanotechnology **20**, 264006 (2009).

[97] S. K. Hämäläinen, N. van der Heijden, J. van der Lit, S. den Hartog, P. Liljeroth, and I. Swart, "Intermolecular contrast in atomic force microscopy images without intermolecular bonds," Phys. Rev. Lett. **113**, 186102 (2014).

[98] A.J. Lee, Y. Sakai, M. Kim, and J.R. Chelikowsky, "Repulsive tip tilting as the dominant mechanism for hydrogen bond-like features in atomic force microscopy imaging," Appl. Phys. Lett. **108**, 193102 (2016).

[99] C.-S. Guo, X. Xin, M.A. Van Hove, X. Ren, and Y. Zhao, "Origin of the contrast interpreted as intermolecular and intramolecular bonds in atomic force microscopy images," J Phys. Chem. C **119**, 14195 (2015).

[100] H. Mönig, S. Amirjalayer, A. Timmer, Z. Hu, L. Liu, O.D. Arado, M. Cnudde, C.A. Strassert, W. Ji, M. Rohlfing, and H. Fuchs, "Quantitative assessment of intermolecular interactions by atomic force microscopy imaging using copper oxide tips," Nature Nanotech. **13**, 371 (2018).

[101] H. Mönig, "Copper-oxide tip functionalization for submolecular atomic force microscopy," Chem. Comm. **1**, 9874 (2018).

[102] Y. Sugimoto, P. Pou, M. Abe, P. Jelínek, R. Pérez, S. Morita and Ó. Custance, "Chemical identification of individual surface atoms by atomic force microscopy," Nature **446**, 64 (2007).

[103] K. Ø. Hanssen, B. Schuler, A J. Williams, T. B. Demissie, E. Hansen, J. H. Andersen J. Svenson, K. Blinov, M. Repisky, F. Mohn, G. Meyer, J.-S. Svendsen, K. Ruud, M. Elyashberg, L. Gross, M. Jaspars, and J. Isaksson, "A combined atomic force microscopy and computational approach for the structural elucidation of breitfussin A and B: Highly modified halogenated dipeptides from thuiaria breitfussi," Angew. Chem. Int. Edit. **51**, 12238 (2012).

[104] Z. Majzik, N. Pavliček, M. Vilas-Varela, D. Pérez, N. Moll, E. Guitián, G. Meyer, D. Peña, and L. Gross, "Studying an antiaromatic polycyclic hydrocarbon adsorbed on different surfaces," Nat. Commun. **9**, 1198 (2018).

[105] T.A. Wesolowski and A. Warshel, "Frozen density functional approach for ab initio calculations of solvated molecules," J. Phys. Chem. **97**, 8050 (1993).

[106] T.A. Wesolowski, S. Shedge, and X. Zhou, "Frozen-density embedding strategy for multilevel simulations of electronic structure." Chem. Rev. **115**, 5891 (2015).

[107] A. Krishtal, D. Sinha, A. Genova, and M. Pavanello, "Subsystem density-functional theory as an effective tool for modeling ground and excited states, their dynamics and many-body interactions," J. Phys. Condens. Matter **27**, 183202 (2015).

[108] A. Lembarki and H. Chermette, "Obtaining a gradient-corrected kinetic-energy functional from the Perdew-Wang exchange functional," Phys. Rev. A **50**, 5328 (1994).

[109] T. Fabien and T. A. Wesolowski, "Link between the kinetic- and exchange-energy functionals in the generalized gradient approximation," Int. J. Quantum Chem. **89**, 441 (2002).

[110] J. P. Perdew, K. Burke, and M. Ernzerhof, "Generalized Gradient Approximation Made Simple," Phys. Rev. Lett. **77**, 3865 (1996).

[111] A. J. Weymouth, T. Hofmann, and F. J. Giessibl, "Quantifying molecular stiffness and interaction with lateral force microscopy," Science **343**, 1120 (2014).

[112] D. Fan, Y. Sakai, and J.R. Chelikowsky, "First-principles study of bond order discrimination in organic molecules using noncontact atomic force microscopy," Nano Lett. **19**, 5526 (2019).

[113] M. Schneiderbauer, M. Emmrich, A.J. Weymouth, and F.J. Giessibl, "CO tip functionalization inverts atomic force microscopy contrast via short-range electrostatic forces," Phys. Rev. Lett. **112**, 166102 (2014).

[114] A. Genova and M. Pavanello, "Exploiting the locality of periodic subsystem density-functional theory: Efficient sampling of the Brillouin zone," J. Phys. Condens. Matter **27**, 499501 (2015).